

https://dspace.org/

A data science framework for mineral resource exploration and estimation using remote sensing and machine learning

Mahboob, Muhammad Ahsan

2024

University of the Witwatersrand, Johannesburg

https://hdl.handle.net/10539/46327

Mahboob, Muhammad Ahsan . (2024). A data science framework for mineral resource exploration and estimation using remote sensing and machine learning [PHD thesis, University of the Witwatersrand, Johannesburg]. WIReDSpace.

Downloaded from a DSpace repository. https://dspace.org/

School of Mining Engineering



UNIVERSITY OF THE
WITWATERSRAND,
JOHANNESBURG

KEY BLOCK THEORY FOR THE MINER: A NOVEL SIMPLIFIED METHOD FOR DETERMINING BLOCK REMOVABILITY

Christiaan van Rooyen (781450)

A research report submitted to the Faculty of Engineering and the Built Environment, University of the Witwatersrand, Johannesburg, in partial fulfilment of the requirements for the degree of Master of Science in Engineering.

Johannesburg, 2023

DECLARATION

I declare that this report is my own, unaided work. I have read the University Policy on Plagiarism and hereby confirm that no plagiarism exists in this report. I also confirm that there is no copying nor is there any copyright infringement. I willingly submit to any investigation in this regard by the School of Mining Engineering and I undertake to abide by the decision of any such investigation.



25 February 2024

Signature of Candidate

Date

ABSTRACT

Rock falls driven by gravity cause the most injuries and deaths in the South African underground mines. Discontinuities such as joints define most rocks that are free to fall. Key block theory describes how to decide if a rock defined by joints can move into an excavated space. Key block analysis requires complex calculations and many iterations to reach such a decision. The complexity of applying key block theory restricts its routine use. Although there are several methods that address some of the shortcomings of key block theory, none address the complexity of its underlying calculations. The main drive of this research project was to find a method to judge rock block removability that is simple enough to enable the routine application of key block theory in mining. The new gravitational removability theorem described in this report satisfied the need for simplicity. A comparison between the gravitational removability method and the edge vector method on many generated blocks yielded a fair correlation in terms of removability, but less so in terms of non-removability. The definition and application of a set of calibrating geometric conditions in conjunction with the gravitational removability method resulted in a perfect accounting of all the synthetic blocks. The gravitational removability method proved effective in identifying rotational removability as well. This research report presents the new gravitational removability theorem, equations to calculate the gravitational removability number and a set of geometric conditions that allows the judgement of removability of a block with no, or minimal calculation.

For my wife, Angelina, whose support, and sacrifice sustained me on this journey, and my children; Christiaan, Angeline and Jostiaan, for whom I do all.

ACKNOWLEDGMENTS

Professor T.R. Stacey, who encouraged me to embark on this journey years ago and was there to provide advise and support throughout, not only as a supervisor, but as a role model and mentor.

My gratitude to my direct manager and executive at Marula mine, Sifiso Mthethwa, for all the patience, support, and the gift of time.

Marula mine, for providing financial support and the opportunity to complete this journey.

And lastly, Megan Balfour, my colleague and friend, who gave me moral support and encouragement when days were sunny and dark alike.

TABLE OF CONTENTS

DECLARATION ii

ABSTRACT iii

ACKNOWLEDGMENTS v

TABLE OF CONTENTS vi

LIST OF FIGURES x

LIST OF TABLES xii

LIST OF APPENDIX FIGURES xii

1 INTRODUCTION 14

1.1 Background 14

1.2 Statement of the Problem 16

1.3 Hypothesis 18

1.4 Research Methodology 18

1.5 Structure of the Research Report 19

2 GEOLOGICAL DISCONTINUITIES 21

2.1 Chapter Introduction 21

2.2 Main Types 21

2.3 Descriptive Parameters 22

2.4 Field Data Collection Methods 23

2.5 Mapping Bias 25

3 A REVIEW OF BLOCK THEORY 26

3.1 Chapter Introduction 26
3.2 Introduction to Key Block Theory 26
3.3 Computational Methods 27
3.3.1 A joint or surface as a plane 28
3.3.2 Planar half-spaces 28
3.3.3 Intersection of two planes 30
3.3.4 The block pyramid 30
3.4 Block Removability 31
3.5 Chapter Discussion 32
4 COMMERCIAL SOFTWARE 35
4.1 Chapter Introduction 35
4.2 JBlock 35
4.3 UnWedge 36
4.4 ROCK3D 37
4.5 3DEC 37
4.6 Chapter Discussion 38
5 ADVANCES IN KEY BLOCK THEORY 40
5.1 Chapter Introduction 40
5.2 Recent Work 40
5.3 Chapter Discussion 46
6 HYPOTHETICAL MODEL 49
6.1 Chapter Introduction 49

6.2 Rationale 49
6.3 Assumptions 59
6.4 Formulation 60
6.5 Example 66
6.6 Chapter Discussion 69
7 EXPERIMENTAL DESIGN 70
7.1 Chapter Introduction 70
7.2 Block Geometry 70
7.3 Edge Vector Method 75
7.4 Data Generation Model 76
7.5 Chapter Discussion 78
8 RESULTS 79
8.1 Chapter Introduction 79
8.2 Data Quality 79
8.3 Base Results 81
8.4 Calibrated Results 82
8.5 Potential Rotation 83
9 DISCUSSION 85
10 CONCLUSION 90
11 RECOMMENDATIONS 93
REFERENCE LIST 94

APPENDIX A: THREE-SIDED BLOCK DATA QUALITY 110

APPENDIX B: FOUR-SIDED BLOCK DATA QUALITY 113

APPENDIX C: FIVE-SIDED BLOCKS DATA QUALITY..... 116

LIST OF FIGURES

Figure 1: FOG-related fatalities, 2003 - 2022 14

Figure 2: FOG fatalities by mechanism, 2016 - 2020 15

Figure 3: FOG injuries by mechanism, 2016 – 2020 15

Figure 4: Joint orientation parameters. 23

Figure 5: Planes forming a tetrahedron. 29

Figure 6: Tetrahedron formed in the planar common space. 29

Figure 7: Block types 31

Figure 8: Four-sided pyramid 33

Figure 9: Example block 43

Figure 10: Range of C (z-component) 50

Figure 11: Random joint network 51

Figure 12: Two-dimensional view of blocks formed above excavation. 51

Figure 13: Two-dimensional side view of blocks formed in slope 52

Figure 14: Range of angles between vectors 53

Figure 15: Two-dimensional block 54

Figure 16: Removable two-dimensional remnant cavity 54

Figure 17: Normal vectors 54

Figure 18: Non-removable two-dimensional block 55

Figure 19: Two-dimensional combination scenario 55

Figure 20: Geometrically constrained four-sided block 57

Figure 21: Geometrically constrained block cross-section 58

Figure 22: Geometrically constrained block detail..... 58

Figure 23: Tall block..... 64

Figure 24: GRN of regular pyramids 64

Figure 25: GRN versus apex height..... 65

Figure 26: Example planes 67

Figure 27: Example tetrahedron..... 67

Figure 28: Example 1 GRN calculation 68

Figure 29: Two-dimensional projection of example tetrahedron 68

Figure 30: Joint fixed pivot points..... 71

Figure 31: Three-sided limit construction 72

Figure 32: Four-sided limit construction 73

Figure 33: Five-sided limit construction..... 74

Figure 34: 3-Sided plot of GRN (EV removable / GRN not removable) ... 84

Figure 35: GRN removable / EV not removable..... 84

Figure 36: Four-sided non-removable conditions..... 87

Figure 37: Outright removable four-sided block 87

Figure 38: Potential rotationally removable four-sided block..... 88

LIST OF TABLES

Table 1: Commercial software license costs 39

Table 2: Symbols 61

Table 3: Example inputs 66

Table 4: Three-sided block joint dip direction ranges 72

Table 5: Four-sided block joint dip direction ranges 73

Table 6: Five-sided block joint dip direction ranges 74

Table 7: Dip direction degrees of freedom 77

Table 8: Possible combinations 77

Table 9: Base comparison 82

Table 10: Calibrated balance sheet 83

LIST OF APPENDIX FIGURES

APPENDIX A

Figure A - 1: Three-sided dip angle histogram 110

Figure A - 2: Three-sided dip direction histogram 110

Figure A - 3: Three-sided half space distribution 111

Figure A - 4: Three-sided intersection distribution 111

Figure A - 5: Three-sided non-removable block 112

Figure A - 6: Three-sided removable block 112

APPENDIX B

Figure B - 1: Four-sides dip angle histogram 113

Figure B - 2: Four-sides dip direction histogram 113

Figure B - 3: Four-sides half space distribution..... 114

Figure B - 4: Four-sided intersection distribution..... 114

Figure B - 5: Four-sided non-removable block..... 115

Figure B - 6: Four-sided removable block 115

APPENDIX C

Figure C - 1: Five-sided dip angle histogram 116

Figure C - 2: Five-sided dip direction histogram..... 116

Figure C - 3: Five-sided half space distribution..... 117

Figure C - 4: Five-sided intersection distribution..... 117

Figure C - 5: Five-sided non-removable block 118

Figure C - 6: Five-sided removable block 118

1 INTRODUCTION

1.1 Background

According to the Minerals Council of South Africa, the total number of fatalities recorded in the South African mining sector during 2022 amounted to 49 of which six were attributed to Falls of Ground (FOG) (Langenhoven, 2023). The contribution of FOG to South African mining fatalities reduced significantly during 2022 as shown in Figure 1. Despite FOG contributing 12% to the total fatalities during 2022, which was the lowest in 20 years, FOG is still the primary cause of fatalities in the mining sector overall. FOG-related incidents caused 36.5% of mining fatalities overall during the 20 years between 2003 and 2022 in the South African mining sector.

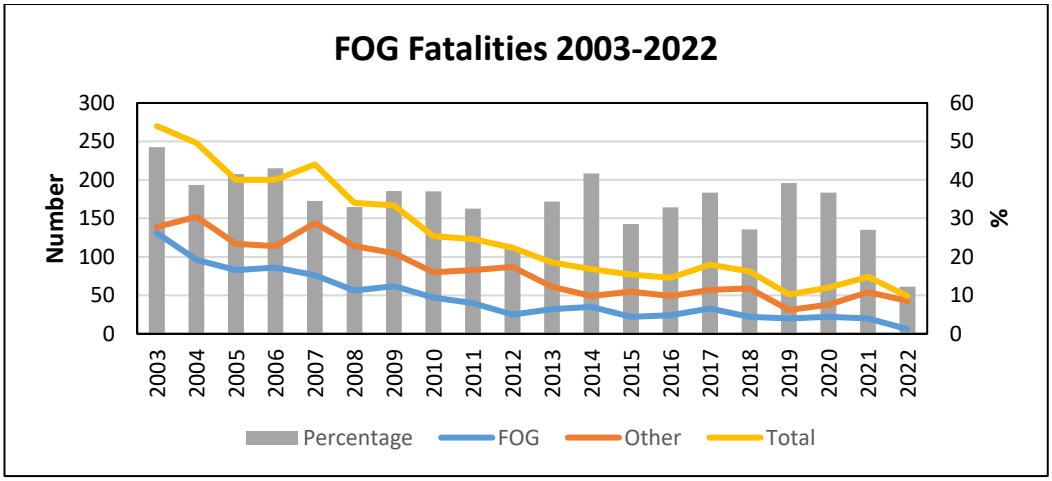


Figure 1: FOG-related fatalities, 2003 - 2022

The South African Department of Minerals and Energy (DMRE) classifies FOG-related injuries and fatalities under two primary mechanisms, namely seismic and gravity. An analysis of the annual reports of the Mine Health and Safety Inspectorate (MHSI) for the five years between 2016 and 2020

indicates that most FOG-related injuries and fatalities, roughly 60% overall, result from gravity as shown in Figure 2 and Figure 3.

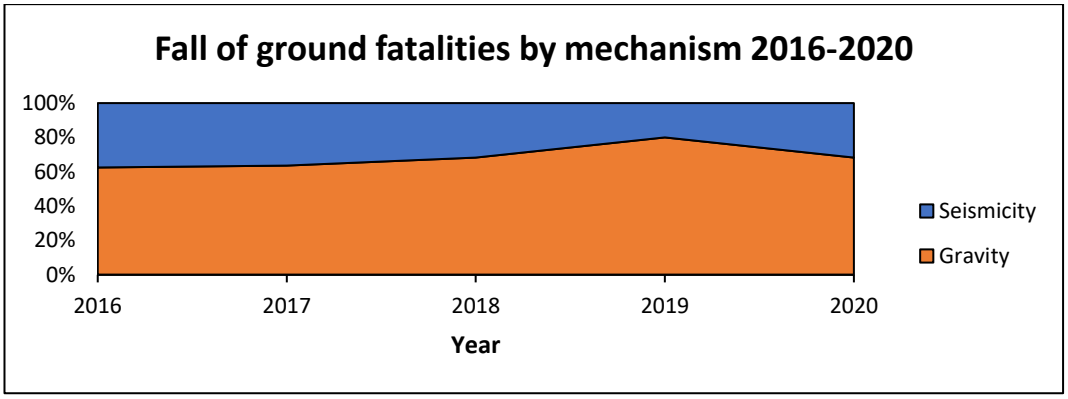


Figure 2: FOG fatalities by mechanism, 2016 - 2020

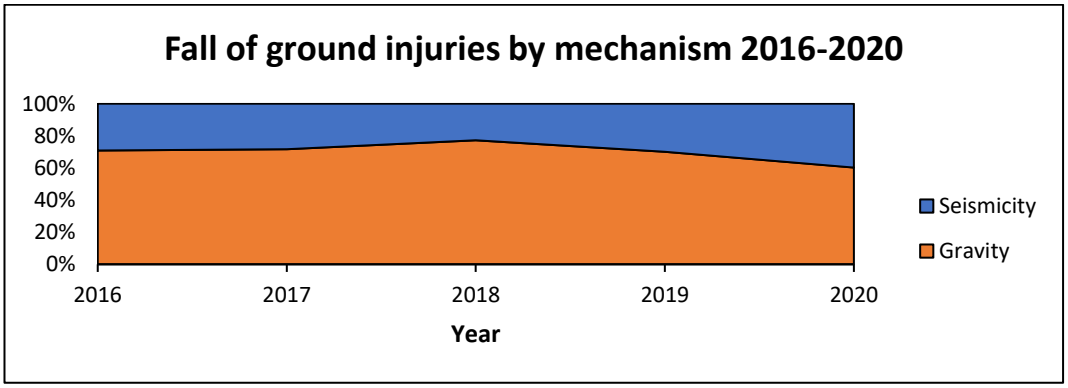


Figure 3: FOG injuries by mechanism, 2016 – 2020

A gravity-driven FOG occurs when a rock is displaced into an excavation with the only force acting on it being gravity. This can only occur when two conditions are met. Firstly, a movable rock must exist and secondly, the movement of such a rock must not be restricted. The first condition relates to the inherent structure and mechanical properties of the rock mass and is therefore difficult to control. The second condition relates to controllable parameters, such as support.

Haile and Jager (1995) concluded in their study of rock mass conditions in the Bushveld Igneous Complex (BIC) that geological structures, especially joints, contribute to the overall ground conditions experienced in underground excavations. The potential to predict hazardous conditions in advance by characterizing the occurrence of jointing was also noted (Haile and Jager, 1995). The conclusion reached by Haile and Jager (1995) still stands today as most rock falls experienced in the BIC are primarily bounded by geological discontinuities.

Goodman, Taylor and Brekke (1968) proposed that a jointed rock mass can be represented as a system of connected blocks (Goodman, Taylor and Brekke, 1968). This concept was later solidified by Goodman and Shi (1985) through the formal introduction of block theory, more popularly referred to as Key Block Theory (KBT), in the field of rock engineering (Goodman and Shi, 1985). The premise of KBT is that removable blocks contribute the most to excavation instability. Given that most of the injuring FOG in the South African mining industry are gravity-driven, KBT is a well-suited approach.

1.2 Statement of the Problem

The application of KBT as a support design tool became popular in the South African mining industry following the release of JBlock, a software package specifically designed for probabilistic key block analysis (Esterhuizen and Streuders, 1998). Several authors, Dunn and Stacey (2008), Dunn, Hagan and Saydam (2010), Joughin et al. (2012a; 2012b), Nezomba (2012), Judeel et al. (2016), Gardner, Bronkhorst and Ayres

(2017), Sewnun et al. (2017), Chikande and Zvarivadza (2018), Khoza et al. (2019), and Netshilaphala and Zvarivadza (2022) have shown the applicability of the probabilistic key block approach (Dunn and Stacey, 2008; Dunn, Hagan and Saydam, 2010; Joughin et al., 2012b; 2012a; Nezomba, 2012; Judeel et al., 2016; Gardner, Bronkhorst and Ayres, 2017; Sewnun et al., 2017; Chikande and Zvarivadza, 2018; Khoza et al., 2019; Netshilaphala and Zvarivadza, 2022). The major disadvantage of the probabilistic approach is that it is not well suited to routine use.

The use of KBT is typically limited to specific projects and is mostly absent in day-to-day mining. Practical constraints such as the cost of software licensing and a certain degree of skill necessary to execute KBT using commercial software contribute to its limited routine application. The computational complexity to determine block removability is daunting and is therefore mostly done through software programming, which places KBT even further out of reach of the miner at the face.

This research aims to develop a method to determine block removability that is sufficiently simple from a computational perspective to promote the utilisation of KBT routinely. The research aims to develop a computational method; hence the primary data will consist of artificially generated blocks that satisfy the experimental design.

A simple method to determine block removability will greatly contribute to reducing FOG-related injuries and fatalities in the South African mining

industry. Should such a method exist some envisaged applications may be the inclusion of key block identification in Triggered Action Response Programs (TARP), pro-active identification of potentially problematic blocks in short-term mine planning and the development of rules of thumb that are easily understood by the miner on the production face.

1.3 Hypothesis

The removability of a convex block, defined by a free surface and several discontinuities, can be judged by considering only the summation of the components of the normal vectors of the constituent joints pointing away from the centroid of the block, relative to the gravitational vector where the contribution of any joint to removability is relative to the angle between the normal vector of the free surface pointing into the rock mass and the normal vector of a joint pointing away from the centroid of the block.

1.4 Research Methodology

A comprehensive review of the methods published to determine block removability will be undertaken for two reasons. Firstly, to gain a sufficient understanding of the computational mechanics involved in determining block removability and secondly, to confirm that a method satisfying the hypothesis of this research does not already exist.

Should such a method not be found the following methodology will be applied:

- A method, consisting of computational considerations and subsequent theorems, which satisfies the hypothesis will be developed and detailed;
- An experimental data set of fictitious blocks will be created and judged for removability using an established method to set up a baseline. The fictitious blocks will then be judged for removability using the new method; and
- A comparison of the performance of the new method relative to the established method will determine the validity of the hypothesis and applicability of the new method.

1.5 Structure of the Research Report

A broad overview of geological discontinuities, measurable parameters and field mapping methods is provided in the next chapter. Chapter 3 describes the rationale, assumptions, relative computational methods, and removability theorems as published in the book *"Block theory and its application to rock engineering"* by Goodman & Shi (1985).

The next two chapters present a comprehensive literature review. Chapter 4 is dedicated to the most widely used KBT-based commercial software packages. Chapter 5 is a critical review of the methods published to determine block removability.

Chapter 6 details the development of the hypothetical model, followed by the experimental design in Chapter 7. The experimental results are presented in Chapter 8 and discussed in Chapter 9. The concluding remarks and subsequent recommendations are given in Chapters 10 and 11.

2 GEOLOGICAL DISCONTINUITIES

2.1 Chapter Introduction

Rock is the medium in which underground mining is executed and unlike other engineering materials, it is not a homogeneous continuum, except at a very small scale. The rock encapsulating the underground mining environment consists of various rock types which are crossed by a multitude of geological structures such as faults, dykes and joints. These geological structures are referred to as discontinuities. The interaction between the rock and discontinuities results in the formation of discrete blocks. The geometry of natural geological discontinuities and the rock blocks that result from their interaction are fundamental to this research project.

This chapter provides a brief overview of the most prominent types of, and relevant parameters of, these discontinuities. Although the main thrust of this research project is not focussed on the detailed statistical characterisation of the rock mass, field data collection methods and sampling biases are also briefly discussed.

2.2 Main Types

The collective term discontinuity refers to any mechanical break in the rock mass with a tensile strength tending towards zero (International Society for Rock Mechanics, 1978). The two most often encountered discontinuities are joints and faults.

The term, joint, refers to a discontinuity displaying no noticeable displacement. Similarly orientated joints form a joint set and a joint system result from the intersection of joint sets. The term, fault, refers to a joint displaying noticeable displacement (International Society for Rock Mechanics, 1978). Within the context of this report the term, joint, will be used throughout to refer to any discontinuity.

2.3 Descriptive Parameters

The International Society for Rock Mechanics (ISRM) (1978) suggested ten parameters that characterize the rock mass and the joints contained in it. These parameters are orientation, spacing, persistence, roughness, wall strength, aperture, filling, seepage, number of sets, and block size (International Society for Rock Mechanics, 1978).

The orientation of a joint refers to its spatial placement and is central to the work of Goodman and Shi (1985). The orientation is expressed in terms of the dip and dip direction as shown in Figure 4.

The dip angle, α, refers to the angle measured between the horizontal and inclined surface. The dip direction, β, refers to the angle measured from the positive y-axis in a clockwise direction to the projection of the dip vector on the x-y plane. The dip vector is a vector pointing in the direction of the steepest dip of an inclined plane. The most used convention is that the positive y-axis coincides with north and the positive x-axis with east (Goodman and Shi, 1985). This convention is maintained in this report.

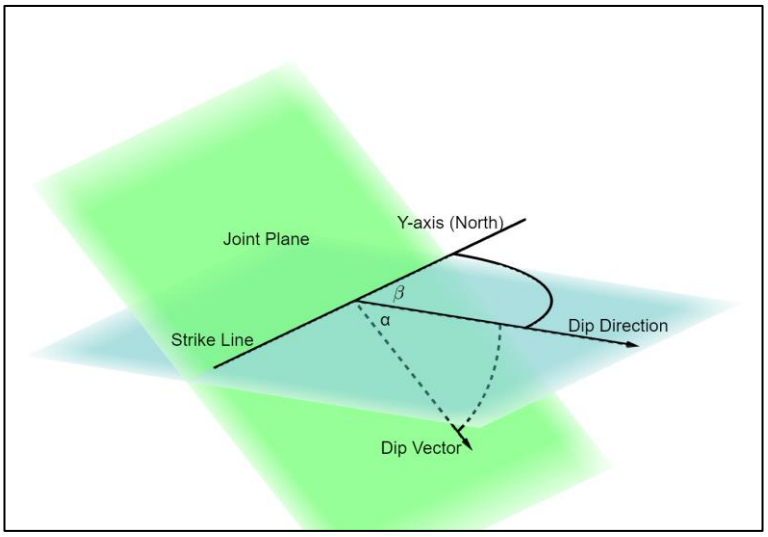


Figure 4: Joint orientation parameters.

2.4 Field Data Collection Methods

The collection of field data, more commonly referred to as joint mapping, is the cornerstone of geotechnical characterisation. Directly measurable joint parameters such as the orientation, spacing and to a certain extent, the trace length are considered primary characteristics. Secondary characteristics are those parameters that require judgement or interpretation such as roughness, wall strength, block size and number of joint sets (Villaescusa, 1992).

Call, Savely and Nicholas (1976) as cited by Villaescusa (1992) classified geological structures as being either main or minor structures depending on their scale (Call, Savely and Nicholas, 1976; Villaescusa, 1992). Main structures are those that are of the same scale as the area of interest, such as major faults and dykes. Minor structures, such as joints, are limited in scale. Call, Savely and Nicholas (1976) observed that the occurrence of

minor structures can be considered infinite from a statistical perspective, hence the necessity for mapping methods (Call, Savely and Nicholas, 1976).

There are various mapping methods described in the literature. Line mapping, as described by Call (1972), involves systematically recording parameters of interest of joints intersecting a taut measuring tape stretched across a rock exposure, such as a face (Call, 1972). Semi-trace length mapping, described by Cruden (1977) and implemented by Priest and Hudson (1981) is akin to line mapping except that only those joint traces above the line are recorded (Cruden, 1977; Priest and Hudson, 1981). Cell, or window, mapping introduced by Mathis (1988) involves defining a rectangular window, or cell and only recording those joints that are observed within it (Mathis, 1988). Methods involving an observation line, such as line and semi-trace length mapping, are referred to as scanline mapping. Scanline mapping is the most common method utilised due to its relative simplicity (Nezomba, 2012).

The world is currently experiencing the fourth industrial revolution, driven by advancements in digital technologies, the inter-connectedness between these technologies and artificial intelligence. These technologies are evolving at an exponential rate (Schwab, 2016). Rock mass characterisation is advancing in step with advances in terms of new methods, miniaturisation, remote sensing, computing, and cost-effectiveness (Blahůt and Racek, 2023). Technologies such as advanced photogrammetry, Light

Detection and Ranging (LIDAR) and point cloud laser scanning are being utilised in the geotechnical domain more often. The works of Herrero et al. (2022), Fernández et al. (2023), Li et al. (2023), Wu et al. (2023), Yan et al. (2023), and Zhao et al. (2023) showcase some of the most recent advancements (Herrero et al., 2022; Fernández et al., 2023; Li et al., 2023; Wu et al., 2023; Yan et al., 2023; Zhao et al., 2023).

Spot mapping, which could be considered as a niche method, involves selectively recording only specific joints and properties that are of interest Brown (2007) as cited by Nezomba (2012) (Brown, 2007; Nezomba, 2012).

2.5 Mapping Bias

Regardless of the method or state-of-the-art equipment employed for joint mapping, errors and inaccuracies do invariably occur. The ultimate validity of any conclusion drawn is directly dependent on the accuracy of the collected data, therefore it is important to be cognisant of the potential errors that can be encountered.

Primary mapping errors occur due to human and instrumentation errors, which can readily be dealt with by training and careful instrumentation selection. The most common sampling errors, or sampling bias, are joint size, orientation, truncation, and censoring (Baecher and Lanney, 1978; Baecher, 1983; Kulatilake and Wu, 1984). Spacing bias occurs when the scanline is not perpendicular to the joints being mapped, which leads to an overestimation of joint spacing (Terzaghi, 1965).

3 A REVIEW OF BLOCK THEORY

3.1 Chapter Introduction

The presence of joints in the rock mass and their contribution to excavation stability are undisputed in the field of rock engineering. Goodman, Taylor and Brekke (1968) concluded that joints contribute significantly to the failure patterns observed in excavations (Goodman, Taylor and Brekke, 1968). This connection between joints and stability led to the creation of the two most well-known rock mass classification systems today, the Rock Mass Rating (RMR) system (Bieniawski, 1973) and the Q-System (Barton, Lien and Lunde, 1974). True removability and kinematic analysis, however, only became tangible with the introduction of KBT by Goodman and Shi (1985).

The advent of KBT has led to many advancements in terms of support and excavation design, which are discussed in a separate chapter. The focus of this chapter is to introduce KBT, summarise the computational methods applied and review the theorems governing block removability. Only the equations most relevant to this research are reproduced.

3.2 Introduction to Key Block Theory

The rock mass is intersected by a multitude of joints which divide it into tessellated blocks resembling a three-dimensional mosaic, referred to as discontinuous rock. This discontinuous rock is constrained in all dimensions, remaining in a state of static equilibrium until disturbed by mining. Mining removes constraints from the rock mass within the void of an excavation,

which allows blocks to move into the excavated space (Goodman and Shi, 1985).

Goodman and Shi (1985) stated that the Kemano tunnel collapse described by Cook, Libby and Madil (1962) was only possible through retrogressive failure and that the Malpasset dam disaster described by Bernaix (1967) was initiated by the movement of a single block (Cook, Libby and Madil, 1962; Bernaix, 1967; Goodman and Shi, 1985). Goodman and Shi (1985) argued that these types of failures cannot occur if such a block, termed a key block, is prevented from moving (Goodman and Shi, 1985).

Goodman and Shi (1985) regarded continuum mechanics as a secondary consideration to the identification of key blocks (Goodman and Shi, 1985). Goodman and Shi (1985) recognised that although the scope of the problem, which is the identification of key blocks, is limited, the following simplifying assumptions would be necessary:

- Joints are perfectly planar;
- Joints extend through the entire rock mass;
- Blocks are rigid; and
- Joints and excavation boundaries are input parameters.

3.3 Computational Methods

The minimum information needed to apply KBT is the dip and dip direction of each joint and excavation surface. The assumption of planarity allows the joints and excavation surfaces to be expressed mathematically as three-

dimensional planes. The equations and their applications that follow are restated from the work of Goodman and Shi (1985) and reflect only those relevant to block removability.

3.3.1 A joint or surface as a plane

The general form of a plane is given by Equation *1*:

$$Ax + By + Cz = D \qquad \text{Equation 1}$$

where A, B and C are the coordinates of the unit vector perpendicular to the plane and D is the perpendicular distance of the plane from the origin. The values of A, B and C are calculated using Equation *2*:

$$\begin{aligned} A &= \sin(\alpha).\sin(\beta) \\ B &= \sin(\alpha).\cos(\beta) \\ C &= \cos(\alpha) \end{aligned} \qquad \text{Equation 2}$$

where α is the dip, between 0° and 90°, and β the dip direction of the joint or surface. The range of the dip angle ensures that C is always positive, hence the normal unit vector will always be the upward normal of the plane.

3.3.2 Planar half-spaces

A plane divides three-dimensional space into an Upper Half-space (UHS) and Lower Half-space (LHS). A point lying above a plane lies in the UHS of the plane and conversely, a point below a plane lies in the LHS of the plane. Mathematically the half-spaces of a plane are expressed as inequalities.

The UHS of a plane is defined by Equation *3*:

$$Ax + By + Cz \geq D \qquad \text{Equation 3}$$

The LHS of a plane is defined by Equation *4*:

$$Ax + By + Cz \leq D \qquad \text{Equation 4}$$

The space common to a combination of the UHS and the LHS of three, or more planes define a block. The common space of the planes shown in Figure 5, for example, forms the tetrahedron shown in Figure 6.

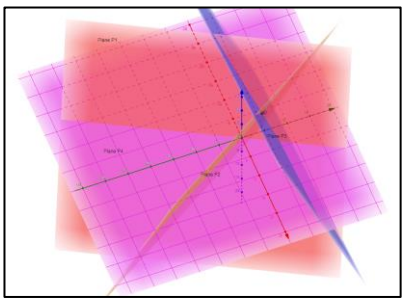


Figure 5: Planes forming a tetrahedron.

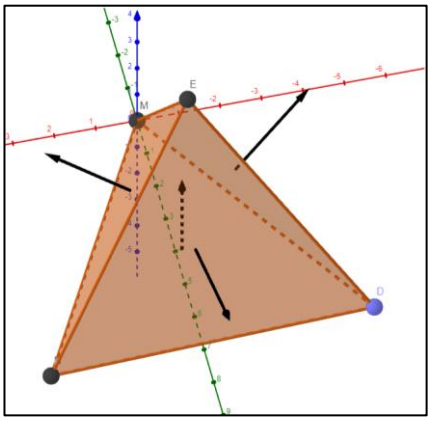


Figure 6: Tetrahedron formed in the planar common space.

3.3.3 Intersection of two planes

An edge to a block forms along the line of intersection of two planes. The unit vector parallel to the line of intersection is the vector cross product of the normal vectors of the two planes. Consider planes A and B with normal vectors $\hat{n}_A = (x_A, y_A, z_A)$ and $\hat{n}_B = (x_B, y_B, z_B)$ respectively. The vector parallel to the line of intersection is given by Equation *5*:

$$I_{AB} = [(y_A z_B - y_B z_A), (x_B z_A - x_A z_B), (x_A y_B - x_B y_A)] \qquad \text{Equation 5}$$

The intersection vector has two directions shown in Equation *6*:

$$I_{AB} = -I_{BA} \qquad \text{Equation 6}$$

3.3.4 The block pyramid

The block pyramid (BP) is central to judging whether a block is removable or not. The BP is constructed by shifting all the planes that define a specific block through the cartesian origin by setting $D=0$ in Equation 3 and Equation 4, for the system of inequalities that defines a specific block.

The intersection vectors $\pm I_{AB}$ must then be calculated for each pair of planes that intersect. Each intersection vector is substituted into the system of inequalities and only those intersection vectors that satisfy all the inequalities define the edges of the BP for any specific block. The BP is empty if no intersection vector satisfies the system of inequalities.

3.4 Block Removability

The fundamental approach of KBT is that the stability of a key block affects the stability of an excavation. Goodman & Shi (1985) classified the geometric configuration of blocks as shown in Figure 7.

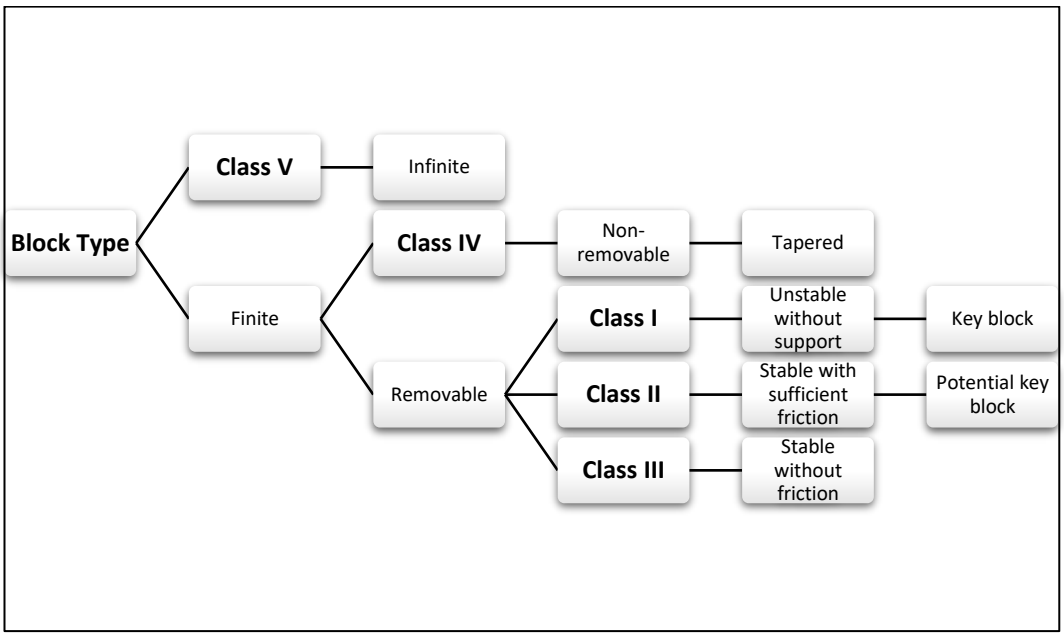


Figure 7: Block types (Goodman and Shi, 1985, p.99)

The definition of a class I or class II block is that the block must be finite, removable, and possibly unstable. The theorem of finiteness is used to determine whether a block is finite. The theorem of finiteness states:

"A convex block is finite if its block pyramid is empty. Conversely, a convex block is infinite if its block pyramid is not empty." (Goodman and Shi, 1985, p.101)

The BP consists of both joints and excavation planes. A Joint Pyramid (JP) is constructed using the same method as for the BP, but only the joint planes are considered. The theorem of removability then states that:

"A convex block is removable if its block pyramid is empty and its joint pyramid is not empty. A convex block is not removable (tapered) if its block pyramid is empty and its joint pyramid is also empty" (Goodman and Shi, 1985, p.108)

Once removability is determined, ultimate stability, or instability, is determined through kinematic analysis. The kinematic analysis considers the equilibrium of stabilising forces acting on a block such as weight, friction, and cohesion. A block is a key block when the stabilising forces are insufficient to counteract the gravitational pull on the block.

3.5 Chapter Discussion

A brief overview of the origin and fundamental concepts of KBT was provided. The computational methods are simple from a mathematical perspective; however, practical execution is an onerous process.

Consider the four-sided pyramid shown in Figure 8. The base represents the hanging wall of an excavation, and the faces are formed by the intersection of four joint planes. The pyramid has five vertices, five faces and eight edges.

The number of potential edges of the BP is given by Equation 7 (Goodman and Shi, 1985) where n is the number of planes.

$$2C_n^2 = n^2 - n \qquad \text{Equation 7}$$

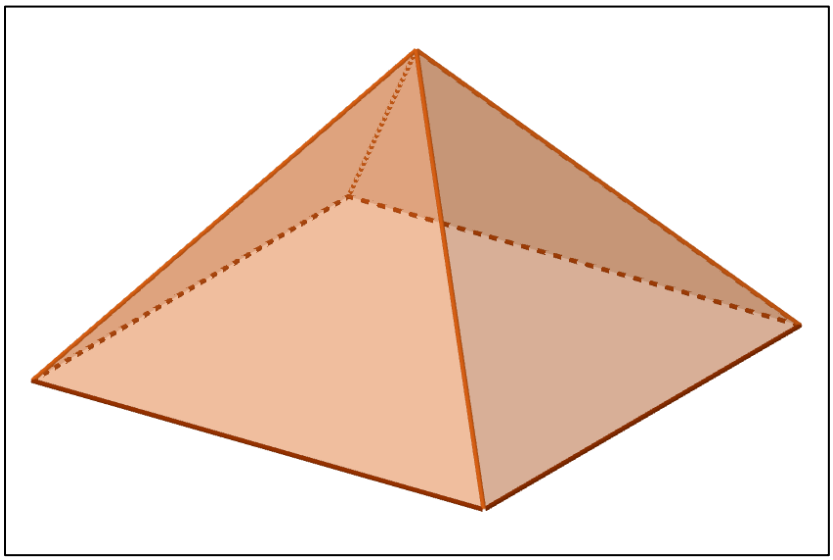


Figure 8: Four-sided pyramid

The BP of the pyramid shown in Figure 8 has 20 possible edges resulting from 10 intersection vectors. The pyramid is defined by five inequalities, hence, finding the edges of the BP will require the substitution of 20 intersection vectors into the system of inequalities, resulting in 100 iterations. Similarly, the edges of the JP will require 12 substitutions in a system of four inequalities, totalling 48 iterations.

Completion of the 48 iterations will only indicate whether a block is finite and, if so, whether the block is removable. The kinematic analysis to determine if the block is a key block requires the block to be considered a polyhedron, for which all the vertices must be defined. A three-dimensional

vertex is formed at the intersection of three planes. Equation *8* is used to determine the number of possible vertices where n is the number of planes.

$$C_3^n = \frac{n!}{3!\,(n-3)!} \qquad \text{Equation 8}$$

The pyramid shown in Figure 8 has ten possible vertices where each vertex must be substituted into the five inequalities that define the block to find the true vertices, resulting in 50 iterations. A true vertex satisfies the system of inequalities. Once the vertices are defined the volume and subsequently, the mass, of the block can be determined, which is essential to conduct the kinematic analysis.

Considering that the number of iterations needed to determine if the pyramid shown in Figure 8 is a key block is potentially more than 200, the application of KBT in practice is nearly impossible without some form of computer code. KBT-based codes written by individuals are described in the literature, but these programs are not readily available to the rock engineer. A few KBT-based software packages, which are discussed in more detail in the next chapter, are commercially available, however, usage of these software packages requires a certain degree of skill and comes at a cost. The regular application of KBT is therefore rarely encountered in practice.

4 COMMERCIAL SOFTWARE

4.1 Chapter Introduction

KBT has, despite the computational complexities discussed, become a cornerstone of rock engineering. In this chapter, the commercial software packages, JBlock, UnWedge, 3DEC and ROCK3D are discussed. Publications by several authors are noted for each software package to demonstrate some of the applications of each software package. The method utilised in each software package to determine block removability or stability is summarised and the cost of each software package is considered.

4.2 JBlock

JBlock is a KBT-based stochastic analysis software package, primarily used in South Africa, developed by G.S. Esterhuizen (Esterhuizen, 2023a). Several authors, including Joughin et al. (2012a; 2012b), Judeel et al. (2016), Gardner, Bronkhorst and Ayres (2017), Sewnun et al. (2017), Chikande and Zvarivadza (2018), Khoza et al. (2019), and Netshilaphala and Zvarivadza (2022) have utilised JBlock effectively in various applications including support design, stable span design and risk quantification (Joughin et al., 2012a; 2012b; Judeel et al., 2016; Gardner, Bronkhorst and Ayres, 2017; Sewnun et al., 2017; Chikande and Zvarivadza, 2018; Khoza et al., 2019; Netshilaphala and Zvarivadza, 2022).

The program generates a specified number of fictitious blocks based on joint set input data. Each block's removability is assessed according to the

method of Goodman and Shi (1985), also referred to as traditional KBT or the Goodman approach (Azarafza and Zhu, 2022). The key blocks are individually tested for stability against a specified support system and the failure statistics are reported (Esterhuizen and Streuders, 1998).

4.3 UnWedge

UnWedge, a software package offered by the Canadian company, Rocscience, can assess the stability of tetrahedral or prismatic wedges in underground excavations (Rocscience, 2023). Publications by Liu, Li and Zhang (2004), Hu et al. (2016), and Zerradi, Lahmili and Souissi (2020) are examples demonstrating the application of the software (Liu, Li and Zhang, 2004; Hu et al., 2016; Zerradi, Lahmili and Souissi, 2020).

A minimum of three joints serves as input. The resulting block is always a wedge and is either tetrahedral or prismatic. The volume of the wedge, the area of each face and the normal vector of each face are calculated as described by Goodman & Shi (1985). The forces acting on the wedge are either active, such as gravity, or passive, such as the capacity of a roof bolt. The individual force vectors are determined and reduced to a resultant active vector and resultant passive vector. The shear strength of each joint is determined using the Mohr-Coulomb, Barton-Bandis or Power curve strength models. The sliding direction of the wedge is then determined as described by Goodman & Shi (1985). The stability of the wedge is reported as a factor of safety considering the active and passive forces (Rocscience, 2022).

4.4 ROCK3D

ROCK3D, supplied by Geo&Soft International, is a KBT-based software package developed for application to rock slopes. The software is not well suited for mining applications but has been utilised for stability analysis of rock slopes as demonstrated by Ferrero, Segalini and Giani (2010) and Quang Minh et al. (2020) (Ferrero, Segalini and Giani, 2010; Quang Minh et al., 2020).

The software follows the key block method described by Goodman and Shi (1985) almost verbatim. The interaction of joints, resulting blocks and subsequent block removability are determined primarily from the stereographic projection methods described by Goodman and Shi (1985) (Geo&soft, 2006).

4.5 3DEC

3DEC, offered by Itasca, differs from the software discussed previously in that it is not a primarily KBT-focused package. The software is a platform for discontinuum modelling based on the Distinct Element Method (DEM) but features an implementation of the linear version of the isolated block stability method developed at Mines Paris Tech by Ghazal, Hadj Hassen and Tijani (2011; 2012) and Ghazal (2013) as cited by Rocscience.com (2013) (Ghazal, Hadj Hassen and Tijani, 2011; 2012; Ghazal, 2013; Rocscience.com, 2013). The software can be utilised as a comparative platform for conceptional simulation, as shown by Wang et al. (2023), for example, or back analysis as demonstrated by Kim, Gratchev and

Balasubramaniam (2015), Wu, Lin and Hu (2018), and Liu et al. (2021) (Kim, Gratchev and Balasubramaniam, 2015; Wu, Lin and Hu, 2018; Liu et al., 2021; Wang et al., 2023).

The isolated block method adopts the traditional assumption of KBT in that joints are perfectly planar, and that movement is only possible along these planes. The premise of the method is to consider the equilibrium of forces before and after excavation. The Mohr-Coulomb criterion is applied to determine the stability of a block by considering the displacement, and subsequent stress vector, at all points in the specific block. Block removability is not directly considered (Ghazal, Hadj Hassen and Tijani, 2011).

4.6 Chapter Discussion

The methods to determine block removability vary between the discussed software packages. JBlock and ROCK3D follow the method by Goodman & Shi (1985) the closest. The isolated block method implemented in 3DEC forgoes block removability in favour of force equilibrium and joint behaviour. The restriction to tetrahedral wedges imposed in UnWedge ensures that the blocks formed are always removable and stability is determined by the effect of active, or driving, forces and passive, or restricting, forces. The assumptions of joint planarity and block rigidity are maintained throughout.

As stated in Section 3.5, the disadvantages common to the discussed commercial software packages are operator skill and cost. A high level of

familiarity with any software package as well as an in-depth knowledge of KBT are necessary to gain any useful outputs. Misinterpretation of, or inaccurate outputs can lead to catastrophic consequences in the production mining environment. The license costs for each of the commercial software packages discussed are summarised in Table 1. The costs reported are correct as stated by the respective distributors and the currency exchange rates on 1 November 2023.

Table 1: Commercial software license costs

Software	License Cost	License Description & Source
JBlock	$1000 R18,742.30	Annual single-user lease (Esterhuizen, 2023b)
UnWedge	$895 R16,774.36	Annual personal subscription (Rocscience.com, 2023)
ROCK3D	€1550 R30,630.58	Perpetual (Geo&Soft, 2023)
3DEC	R215,660.00	Annual web license (Groundwork Consulting, 2023)

The disadvantages discussed see the application of KBT in mining restricted to specific projects executed by either consultancies or researchers.

5 ADVANCES IN KEY BLOCK THEORY

5.1 Chapter Introduction

The collection of joint data, traditional KBT and commercial software based on KBT, either entirely or in part, was discussed in the preceding chapters. There have been many advances made in KBT since its introduction by Goodman and Shi (1985). The main research themes that arise from literature are block identification, such as the recent work by (Yan et al. (2023) and Zhu, Azarafza and Akgün (2022), and block stability, such as the recent work by Zerradi et al. (2023) and Chen et al. (2003) (Chen et al., 2003; Zhu, Azarafza and Akgün, 2022b; Yan et al., 2023; Zerradi, Souissi and Larabi, 2023).

The terms block removability and block stability may appear to be similar in meaning but in the context of KBT, these are very different. A block is removable if its geometry allows it to move out of the rock mass through a free surface or surfaces, but removability does not automatically imply instability. Conversely, a non-removable block is inherently stable as well. The most recent advances in KBT are scrutinized in this chapter, specifically in terms of how block removability is determined.

5.2 Recent Work

Yan et al. (2023) presented a comprehensive methodology utilising photogrammetric structural data obtained from the use of an Unmanned Aerial Vehicle (UAV) to identify potential blocks through graph theory. Heliot (1988) first represented the mapped joint traces and their intersections as

graphs (Heliot, 1988). Yan et al. (2023) identified potential convex blocks by applying a depth-first-search algorithm on the intersection vertices of joints represented as graphs. Once the real blocks were identified removability was determined through edge vector analysis described by Goodman and Shi (1985) as cited by Yan et al. (2023) (Goodman and Shi, 1985; Yan et al., 2023).

The Edge Vector (EV) method was not described in the chapter on traditional KBT; hence a short description is offered for context. EV analysis simply states that a block is removable when none of the constituent joints constrains its movement path. This condition is determined mathematically through the scalar product of the inwards normal of any joint plane and any intersection vector between two joint planes of which the block is comprised. A positive result implies freedom of movement. A block is removable if this condition is upheld for all the joints and intersection vectors of a block (Warburton, 1981; Goodman and Shi, 1985; Yan et al., 2023). The EV method is discussed in more detail in Chapter 7.

Wang et al. (2023) presented a proposed new method to determine the removability of blocks with concave free surfaces by subdivision into an assembly of convex blocks. Removability, however, was determined through traditional KBT. The block stability assessment considers inter-block forces and rotation, which is not considered in traditional stability analyses (Wang et al., 2023).

Zerradi et al. (2023) investigated planar, wedge and toppling failure using the slope mass rating and KBT (Zerradi et al., 2023). Zerradi, Souissi and Larabi (2023) presented a methodology for the selection of the maximum stable slope angle for an open pit mine (Zerradi, Souissi and Larabi, 2023). In both cases block removability was determined through traditional KBT, utilising the stereographic projection method (Zerradi et al., 2023; Zerradi, Souissi and Larabi, 2023) .

Zhu, Azarafza and Akgün (2022) proposed an algorithm for classifying key blocks and judging their stability. The primary joint data was obtained from processing high-quality photographs of rock slopes. The removability of blocks was determined by utilising traditional KBT (Zhu, Azarafza and Akgün, 2022a).

Cheng et al. (2021a; 2021b) proposed an algorithm to address a common shortcoming of traditional KBT, which is the consideration of non-convex blocks. A notable deviation from KBT presented by Cheng et al. (2021a; 2021b) relates to the theorem of finiteness. The assumption made by Cheng et al. (2021a; 2021b) is that all real blocks are finite and therefore the check for finiteness can be omitted when determining removability (Cheng et al., 2021a; 2021b). This assumption is correct. The block formed above the grey plane representing the free surface in the hanging wall shown in Figure 9 is finite but not removable. The theorem of finiteness, however, classifies this block as infinite since the block pyramid is not empty. The non-convex block

is addressed by subdividing the block into convex blocks. Block removability is determined by traditional KBT (Cheng et al., 2021a; 2021b).

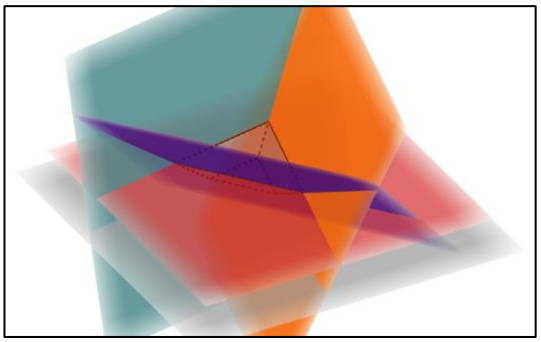


Figure 9: Example block

Wang et al. (2021) introduced the Generalised Joint Pyramid (GJP) method to cater for both convex and non-convex blocks. The GJP method introduces two refinements to traditional KBT. Firstly, convex, and non-convex blocks are not considered separately and, secondly, only essential joints are considered. A joint is redundant if its intersection with any other joint is not an edge of the GJP. Essential joints are identified by an implementation of the union search method by Cormen et al. (2009) as cited by Wang et al. (2021) (Cormen et al., 2009; Wang et al., 2021). Block removability is determined by an application of the stereo-analytical analyses introduced by Zhang and Kulatilake (2003) as cited by Wang et al. (2021) (Zhang and Kulatilake, 2003; Wang et al., 2021). A non-empty GJP implies a removable block and an empty GJP implies a non-removable block (Wang et al., 2021).

Zhang et al. (2020) introduced a methodology for stability analyses utilising the General Block (GB) method described by Yu et al. (2005), Yu, Xue and Chen (2007), and Zhang and Qing-chun (2010) (Yu et al., 2005; Yu, Xue and Chen, 2007; Zhang and Qing-chun, 2010; Zhang et al., 2020). The methodology is primarily focused on the generation of a three-dimensional block model and the identification of blocks. Block removability is not determined separately from the stability analysis. The stability analysis is based on the inward normal vectors, the resultant block movement vector and the resultant force vector (Zhang et al., 2020). This method is very similar to the edge vector method described previously.

The research conducted by Chen et al. (2019) was focused on addressing non-removable blocks and blocks that are completely defined by joints, which are usually assumed to be stable by key block analysis, such as the GB method introduced by Yu et al. (2005), Yu, Xue and Chen (2007), and Zhang and Qing-chun (2010) (Yu et al., 2005; Yu, Xue and Chen, 2007; Zhang and Qing-chun, 2010; Chen et al., 2019). Chen et al. (2019) postulated that these ignored blocks may become unstable later as mining introduces new free surfaces. Chen et al. (2019) introduced the minimum fixed area consideration which aimed at determining the minimum area by which a block must be attached to the rock mass to remain stable. The minimum fixed area is dependent on the tensile, compressive and shear strength of the rock. An infinite block will remain stable if these strengths are not exceeded by the loading environment (Chen et al., 2019).

Wu et al. (2017) presented the Centroid Sliding Pyramid (CSP) as an improvement to traditional KBT in that non-convex blocks are analysed more efficiently, and the removability pyramid only considers those joints intersecting the free surface (Wu et al., 2017). The CSP is a conical region representing all possible movement vectors of the centroid of a block. The CSP is a function of each pair of sliding vectors of each free domain. The conic angle of each CSP indicates the removability of the block (Wu et al., 2017).

Zheng, Xia and Yu (2015) stated that non-removable blocks may pose a greater risk than removable blocks. The main criticism of KBT is that due to the assumption of block rigidity, blocks are analysed independently from the rock mass, while fracturing of intact rock may cause a stable block to become mobile (Zheng, Xia and Yu, 2015). The central theme of this method is the identification of intact rock bridges and whether such a bridge will remain stable.

Yarahmadi, Bafghi and Verdel (2003) introduced the Key Group Method (KGM) for two-dimensional modelling and Noroozi, Jalali and Yarahmadi-Bafghi (2012) later expanded the KGM to three dimensions by allowing for iterative rock mass analysis (Yarahmadi Bafghi and Verdel, 2003; Noroozi, Jalali and Yarahmadi-Bafghi, 2012). Block removability is determined through the Goodman & Shi (1985) approach; however, the rock mass is divided into groups, of which each group must contain a key block. With each iteration unstable blocks are removed, and the rock mass is re-

grouped. This process is repeated until a stable state is achieved (Yarahmadi Bafghi and Verdel, 2003; Noroozi, Jalali and Yarahmadi-Bafghi, 2012).

Zhang and Kulatilake (2003) presented the stereo-analytical method to determine block removability. This method is a hybrid between stereographic projection and analytical methods. The intersection points between joints are determined to be either positive or negative. The block is then represented as a collection of intersection points in matrix form. Inspection of the matrix rows is used to determine the emptiness of the joint pyramid and block pyramid. The theorems of finiteness and removability by Goodman and Shi (1985) are then applied to determine removability (Zhang and Kulatilake, 2003).

5.3 Chapter Discussion

The determination of block removability is the central theme of KBT without which, no further analyses are possible. The two fundamental approaches when considering block removability are vector analysis and stereographic projection. Vector-based methods rely on the planar normal vectors while stereographic methods rely on focal point projection (Wang et al., 2021).

The methods discussed in this chapter aimed to improve judgement of block removability. These methods are the stereo-analytical method (Zhang and Kulatilake, 2003), the key-group method (Yarahmadi Bafghi and Verdel, 2003), unified analysis (Zheng, Xia and Yu, 2015), centroidal sliding

pyramid (Wu et al., 2017), minimum fixed area (Chen et al., 2019) and most recently, the generalised joint pyramid method (Wang et al., 2021).

The principal assumptions of KBT, which are joint and free surface planarity and block rigidity are maintained throughout, except for the unified and minimum fixed area methods. The motivation for the development of a new method or improvement on an existing method has been to address some shortcomings of the original KBT methods or applicability.

The generalised joint pyramid method was aimed at generalising the removability analyses for both convex and non-convex blocks and improving computational efficiency by only considering essential joints (Wang et al., 2021). The concept of the minimum fixed area was focused on the stability of non-removable blocks to address the inadequacy in the three-dimensional graphics processing of the GeneralBlock program (Chen et al., 2019). A description of the GeneralBlock program was given by Xia et al. (2015).

The centroid sliding pyramid addressed the subdivision of non-convex blocks more efficiently and simplified removability determination by only considering joints intersecting the free surface (Wu et al., 2017). The unified analysis method considered the stability of non-removable blocks by considering the mechanical failure of rock bridges that constrain such blocks (Zheng, Xia and Yu, 2015).

The key group method allowed for considering the stability of multiple blocks simultaneously, which showed improved processing efficiency as compared to the distinct element method (Yarahmadi Bafghi and Verdel, 2003). The stereo-analytical method was aimed at addressing the computational complexity regarding the removability of blocks, convex or non-convex, defined by more than four joints (Zhang and Kulatilake, 2003).

The methods discussed, although some claim to be a simplification in one area or another, are still computationally complex, which necessitates incorporation into some code to be utilised. For instance, the most recent work by Zhu, Azarafza and Akgün (2022), Yan et al. (2023), Zerradi et al. (2023) and Zerradi, Souissi and Larabi (2023) presented methodologies which make use of established removability methods but only as a step in a procedure. The general direction of KBT is becoming more focused on data collection through state-of-the-art digital technologies, automated block identification and more realistic rock mass stability modelling. Unfortunately, the more advanced KBT becomes the further the benefits move away from the production face where time is limited, and adoption of technology is slow.

6 HYPOTHETICAL MODEL

6.1 Chapter Introduction

This chapter describes the rationale and formulation of the proposed new method to determine block removability following the stated hypothesis.

6.2 Rationale

The focus of the proposed method is to determine block removability through vector analysis. The research hypothesis is restated to provide context:

"The removability of a convex block, defined by a free surface and several discontinuities, can be judged by considering only the summation of the components of the normal vectors of the constituent joints pointing away from the centroid of the block, relative to the gravitational vector where the contribution of any joint to removability is relative to angle between the normal vector of the free surface pointing into the rock mass and the normal vector of a joint pointing away from the centroid of the block."

Section 3.3.1 showed that a joint, or free surface, is represented mathematically as a three-dimensional plane. A plane is completely defined by its dip and dip direction, which are used to calculate the coordinates of the normal vector to the plane through substitution in Equation *2*. Since the measurement range for the dip of a joint or free surface is always between zero and 90° the normal vector calculated will always have a positive z-

component between zero and one, hence be the upward normal vector as shown in Figure 10.

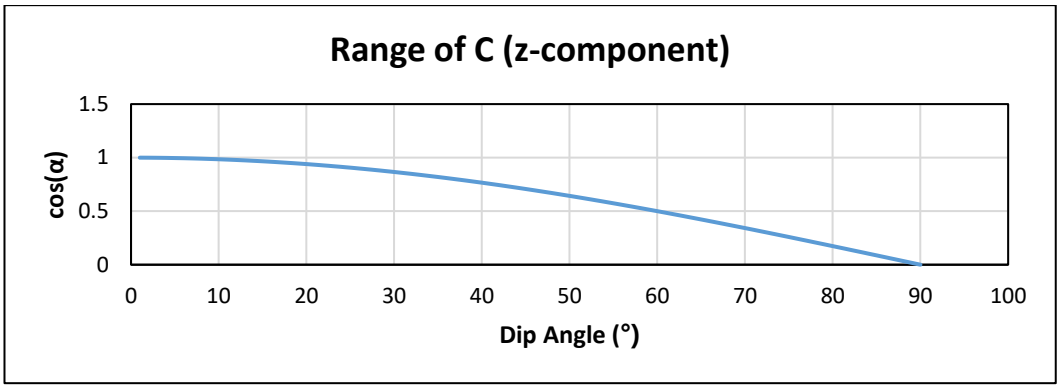


Figure 10: Range of C (z-component)

The fact that the normal vector will always be the upward normal is important when considering the planar half-space. If a block lies in the UHS of the plane the calculated normal vector will be in the direction of the block, referred to as the inwards normal. Conversely, if a block lies in the LHS of a plane the calculated normal vector will be in the direction of the rock mass, referred to as the Rock Mass Vector (RMV). The normal vector of a free surface, when considering the hanging wall, will always be directed into the block, but also into the rock mass.

Joints divide the rock mass into a collection of discrete blocks. Each block is held in place by the constraint provided by its neighbours. The two-dimensional side view of an arbitrary joint network shown in Figure 11 illustrates this scenario.

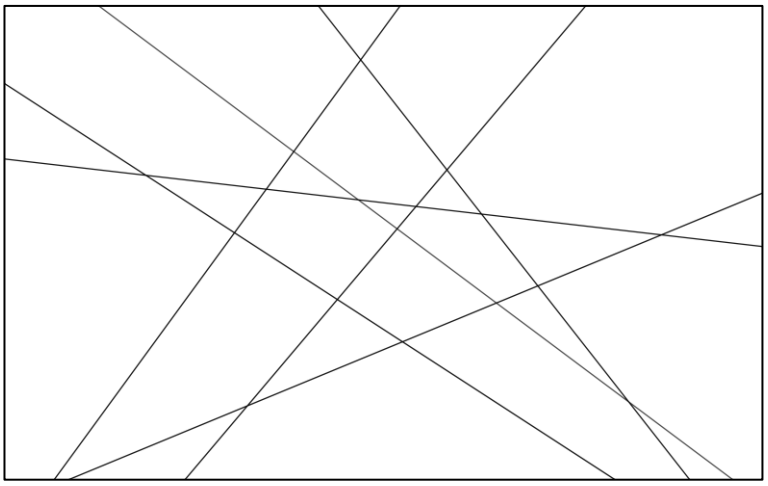


Figure 11: Random joint network

Several blocks form where the joints intersect, but in the absence of a free surface, these blocks are inherently part of the rock mass. The introduction of a free surface results in blocks that could potentially move into an excavation. The red line shown in Figure 12 represents a free surface, the hanging wall in this case, introduced into the rock mass which illustrates this concept.

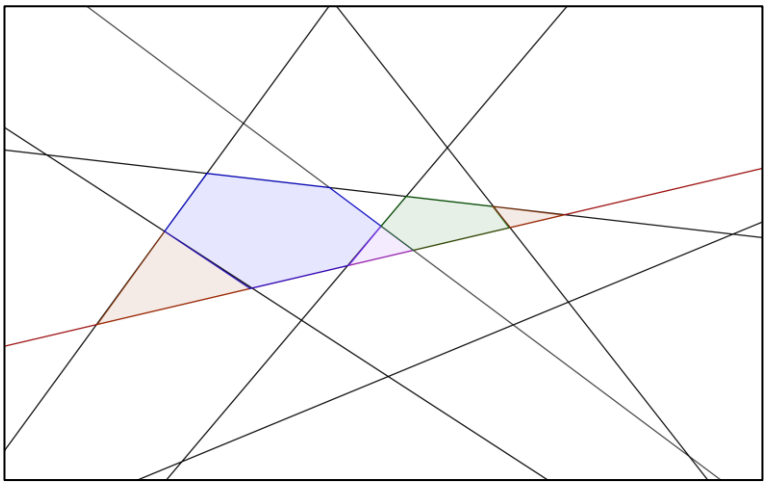


Figure 12: Two-dimensional view of blocks formed above excavation.

The orientation of the free surface relative to the joints affects the blocks formed as well as the removability of these blocks. Considering the same free surface shown in Figure 12 as a slope, the blocks that could potentially move are quite different as shown in Figure 13.

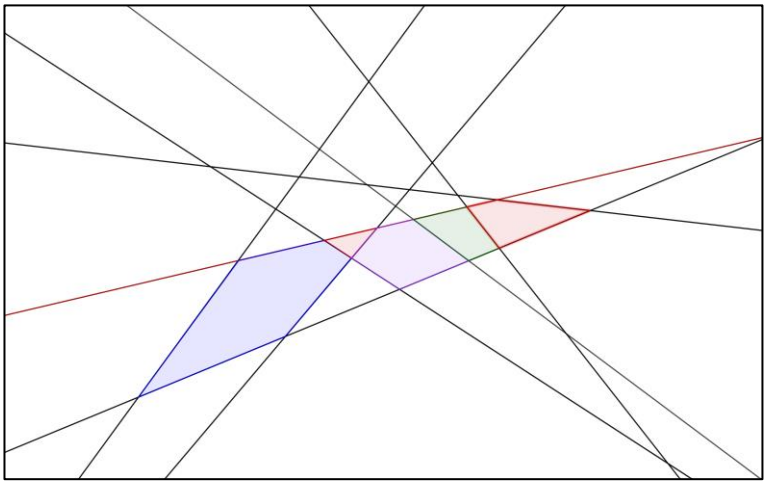


Figure 13: Two-dimensional side view of blocks formed in slope.

The orientation of the free surface relative to the excavated space is therefore the most important factor when considering block removability. The second most important factor is the relative orientation between the free surface and each joint that defines a block.

The orientational relationship between a free surface and any joint can be described by the angle between the RMV of the free surface and the RMV of a joint. The dot product of these the two vectors gives an indication whether this angle is more or less than 90°. Equation *9* gives the formula for calculating the angle using the dot product, where θ is the angle between any two vectors $\mathbf{a}$ and $\mathbf{b}$.

$$\cos\theta = \frac{a.b}{|a||b|}$$ Equation 9

Equation *10* yields the dot product of two vectors, $a = (x_a, y_a, z_a)$ and $b = (x_b, y_b, z_b)$.

$$a.b = (x_a x_b).(y_a y_b).(z_a z_b)$$ Equation 10

Considering that Equation *2* produces a unit vector, Equation *9* simplifies to Equation *11*.

$$\cos\theta = \hat{a}.\hat{b}$$ Equation 11

The maximum angle between two vectors is 180°, or π radians, which implies that the two vectors are directionally exactly opposite. The range of values of $\cos\theta$ is shown in Figure 14.

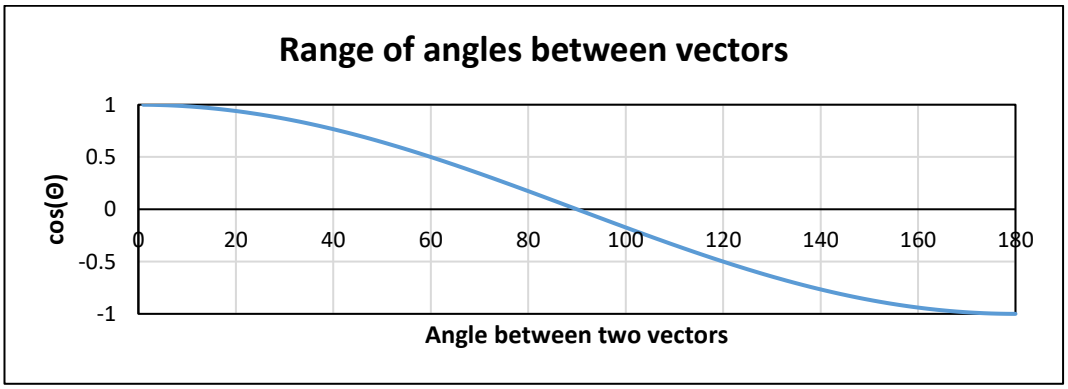


Figure 14: Range of angles between vectors

Consider the two-dimensional triangular block formed by three lines in Figure 15, which is removable. The block is the region where the half-planes coincide. In this case, it is the lower half-planes of the joints (blue) and the

upper half-plane of the free surface (red). Removal of the block results in a remnant cavity as shown in Figure 16.

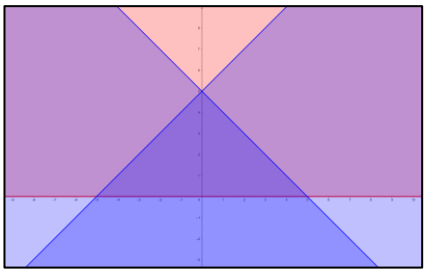


Figure 15: Two-dimensional block

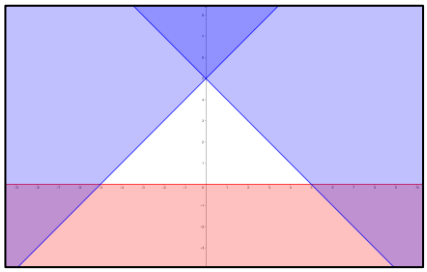


Figure 16: Removable two-dimensional remnant cavity

The RMV for the three lines are shown in Figure 17.

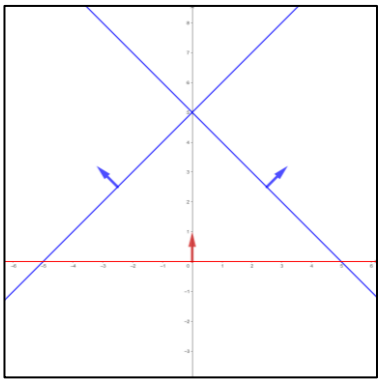


Figure 17: Normal vectors

From Figure 17 the angle between the RMV of the free surface and both joints is less than 90°. A non-removable scenario is shown in Figure 18.

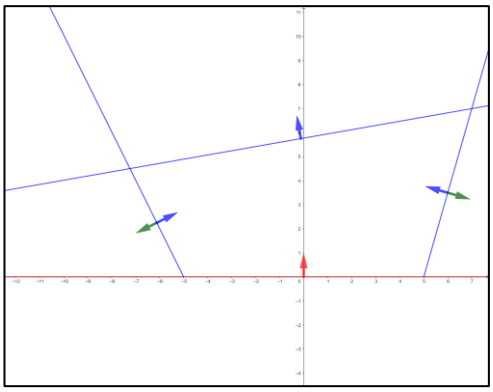


Figure 18: Non-removable two-dimensional block

In the non-removable scenario, the RMV (green) of the joints (blue) do not necessarily coincide with the upward normal vectors (blue). A combination of joint orientations, as shown in Figure 19, is also possible.

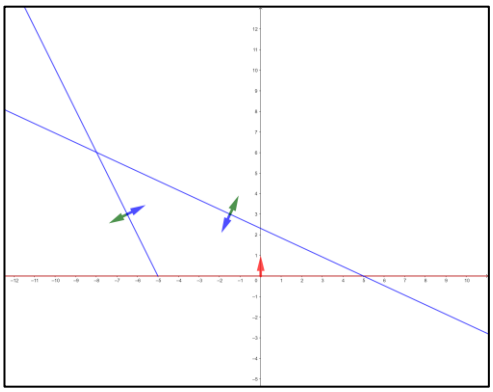


Figure 19: Two-dimensional combination scenario

The scenarios presented in Figure 17, Figure 18 and Figure 19 demonstrated that the angle between the RMV of a free surface and that of a joint is an indication of whether a block will be constrained along that joint.

An angle of less than 90° will contribute to removability while an angle exceeding 90° will constrain block movement. This concept alone, however, is not sufficient to determine removability.

Gravity is the principal force that drives block movement. The unit vector for gravity in cartesian space is $\hat{\mathrm{g}} = (0,0,-1)$. The gravitational vector, although it represents a force, can be related to the geometric analysis through Newton's third law of motion which states that any applied force is counteracted by an equal force in the opposite direction of the applied force. It then stands to reason to surmise that a block is removable when there is insufficient geometric constraint to maintain its static equilibrium under gravitational load.

A free surface is not a physical entity, it is merely a space into which a block may move, therefore the free surface is not considered further beyond classifying a joint as contributing to or constraining movement. The practical interpretation of a constraining joint is that there is intact rock between the face of the block and the free surface. Conversely, a contributing joint has no intact rock between the face of the block and the free surface.

Wu et al. (2017) introduced the concept of a "free domain" to account for the concave corners of a block. Only those joints intersecting a free surface are considered in the determination of removability (Wu et al., 2017). The "free domain" concept will be included in the proposed new method.

Scenarios arise in practice where a block is non-removable based only on the physical configuration of its constituent joints. Goodman & Shi (1985) stated that a block is removable when it can be moved in some direction that does not cause the block to “collide” with adjacent rock (Goodman and Shi, 1985). Consider the block formed by a free surface and four joints shown in Figure 20.

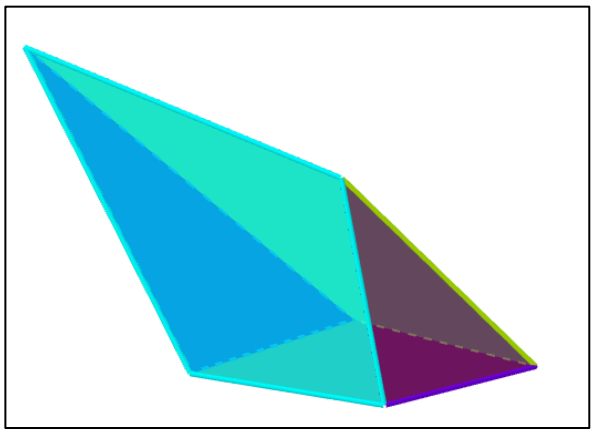


Figure 20: Geometrically constrained four-sided block

At face value, the block appears to be removable, but it is not. A section plane cut through the block yields the side-view polygon, PNSR, shown in Figure 21. The block lies in the UHS of segment PS and the LHS of segment RN. The dip angle of segment PS is shallower than the dip angle of segment RN as shown in Figure 22. Any movement of the block will result in a “collision” as described by Goodman & Shi (1985) with the rock mass along segment RN, effectively constraining the movement of the block (Goodman and Shi, 1985).

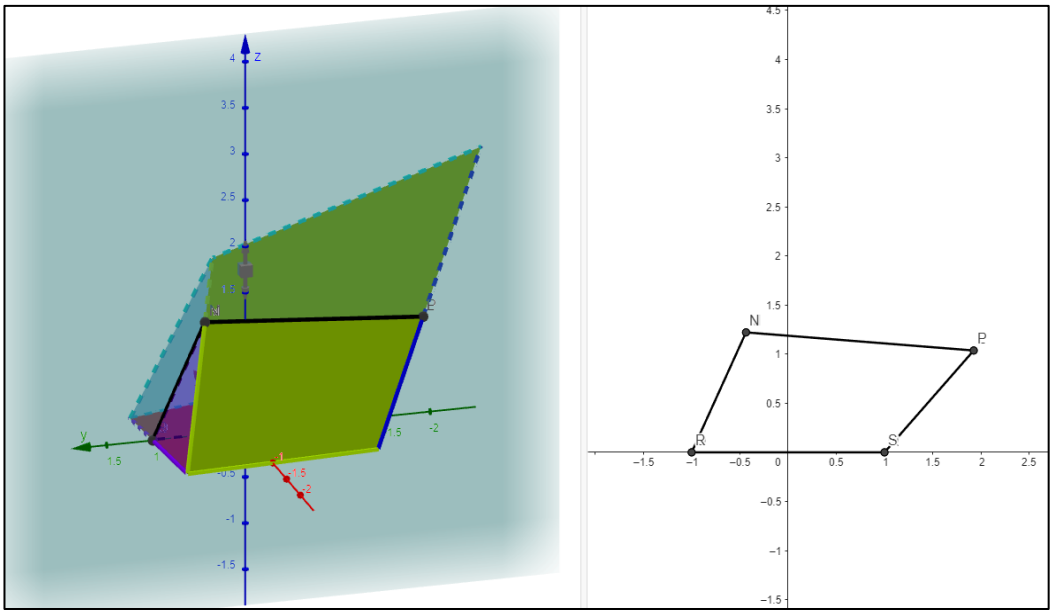


Figure 21: Geometrically constrained block cross-section

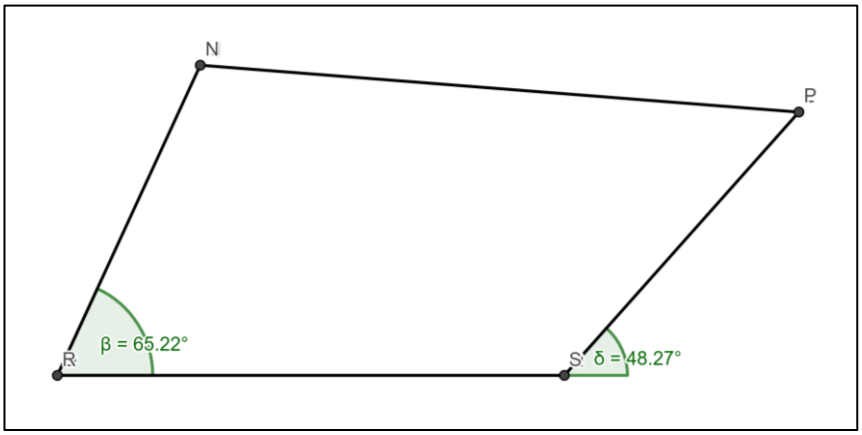


Figure 22: Geometrically constrained block detail

The concept of geometric constraint is important in the context of this research. A set of “rules of thumb” concerning geometric constraints will be helpful in the sense that non-removable blocks could be identified without the need for any calculations. This concept will be explored further once the data models are completed.

The rationale and reasoning leading up to the proposed method were discussed in this section. The base assumptions and mathematical formulation of the proposed method are detailed hereafter.

6.3 Assumptions

The following assumptions of KBT as set out by Goodman & Shi (1985) are maintained by the proposed method:

- Joints and free surfaces are perfectly planar;
- Blocks are entirely bounded by free surfaces and existing joints;
- Blocks are rigid; and
- The dip, dip direction and half-spaces of the constituent planes are input quantities.

The following concepts from other authors are also incorporated into the proposed method:

- The test for finiteness is discarded (Cheng et al., 2021a; 2021b);
- Only those joints intersecting the free surface are considered (Wu et al., 2017);
- The actual spatial location of each constituent plane is a secondary consideration to the relationship between the various unit vectors as shown by the construction of the block and joint pyramids (Goodman and Shi, 1985); and
- Only the gravitational movement direction of a block is relevant to determining a block's removability, hence the gravitational unit vector satisfies the removability analysis (Warburton, 1981).

The final assumption is that the proposed method is only applied to those blocks that have not been discarded outright as removable or non-removable based on geometric conditions.

6.4 Formulation

The following spatial orientation conventions are adopted:

- North coincides with the positive y-axis;
- East coincides with the positive x-axis;
- The dip is measured as the angle below the horizontal to a maximum of 90°;
- Dip direction is measured clockwise from north; and
- Up is in the direction of the positive z-axis.

The first step in the execution of the proposed method is to determine the upwards normal unit vectors for the constituent planes. Equation *2* is used to calculate the components of the upward normal unit vector represented by Equation *12*:

$$\hat{n} = A\hat{i} + B\hat{k} + C\hat{j} \qquad \text{Equation 12}$$

Once the upwards normal unit vectors are calculated the RMV of each plane must be determined. Symbols relative to the proposed method are stated in Table 2.

Table 2: Symbols

Symbol	Meaning
$\hat{n}_{Ji}$	Upward normal unit vector of joint i
$\hat{n}_{FS}$	Upward normal unit vector of the free surface
$\hat{r}_{Ji}$	Rock mass vector of joint i
$r_{Ji}z$	z-coordinate of $\hat{r}_{Ji}$
$\hat{r}_{FS}$	Rock mass vector of the free surface
$r_{FS}z$	z-coordinate of $\hat{r}_{FS}$
S_{Ji}	Absolute value of $r_{Ji}z$ constraining movement
G_{Ji}	Absolute value of $r_{Ji}z$ contributing to movement
RC	Total constraint
RG	Total contribution
GRN	Gravitational removability number

The orientation of the RMV for the free surface is determined by applying Lemma 1 and the RMV for each joint by applying Lemma 2.

Lemma 1: *If the rock mass is situated in the UHS of the free surface, then $\hat{r}_{FS} = \hat{n}_{FS}$. Conversely, if the rock mass is situated in the LHS of the free surface, then $\hat{r}_{FS} = -\hat{n}_{FS}$.*

Lemma 2: *If a block is situated in the LHS of joint, i, then $\hat{r}_{Ji} = \hat{n}_{Ji}$. Conversely, if a block is situated in the UHS of joint, i, then $\hat{r}_{Ji} = -\hat{n}_{Ji}$.*

The next step is to classify each joint as contributing to or constraining removability. Considering Equation *11* and Figure 14, Lemma 3 is used to

classify each joint. A special case arises when the RMV of the free surface and the RMV of a joint are perpendicular to each other, which is addressed by Lemma 4.

Lemma 3: *Joint, i, constrains movement when* $\hat{r}_{FS}.\hat{r}_{Ji} < 0$, *then* $S_{Ji} = |r_{Ji}z|$. *Joint, i, contributes to movement when* $\hat{r}_{FS}.\hat{r}_{Ji} > 0$, *then* $G_{Ji} = |r_{Ji}z|$.

Lemma 4: *When* $\hat{r}_{FS}.\hat{r}_{Ji} = 0$ *and the dip angle of the free surface is not zero joint, i, constrains movement when* $r_{Ji}z < 0$, *then* $S_{Ji} = |r_{Ji}z|$. *Joint, i, contributes to movement when* $r_{Ji}z > 0$, *then* $G_{Ji} = |r_{Ji}z|$.

The total constraint against movement, RC, is calculated by a summation of all the absolute values of the z-components of the joints constraining movement. The total contribution to movement, RG, is calculated by a summation of all the absolute values of the z-components of the joints contributing to movement. The gravitational removability number, GRN, is calculated using Equation *13*.

$$\mathrm{GRN} = (1 + \mathrm{RC}) - \mathrm{RG} \qquad \text{Equation 13}$$

The gravitational removability theorem then states that:

A block formed by the intersection of a free surface and several joints is not removable when its gravitational removability number is greater than zero. A block is removable when its gravitational removability number is less than zero.

The scenario where the joints are not constraining but have steep dip angles introduces a point of contention when considering the gravitational removability number. Figure 23 illustrates a tall block formed by steeply dipping joints (green), resulting in a width-to-height ratio of 1:5. Such a block would typically be classified as a tapered block according to Goodman and Shi (1985) (Goodman and Shi, 1985). Yow (1985) also concluded that the magnitude of the effect of block “slenderness” is comparable to that of the shear strength of the joints (Yow, 1985).

The GRN was calculated for a set of pyramids with regular polygons as bases, ranging from three to six sides and varying the dihedral angles, which are equal to the dip angles, to produce Figure 24. Figure 25 was produced by determining the apex height of each pyramid and comparing it to the associated GRN for each dip angle. The “slenderness” effect is demonstrated in both instances. Slender blocks, however, rarely occur in underground mining as the blocks are often “trimmed” by a parting plane, such as the Chromatite markers found in the hanging wall of most platinum mines.

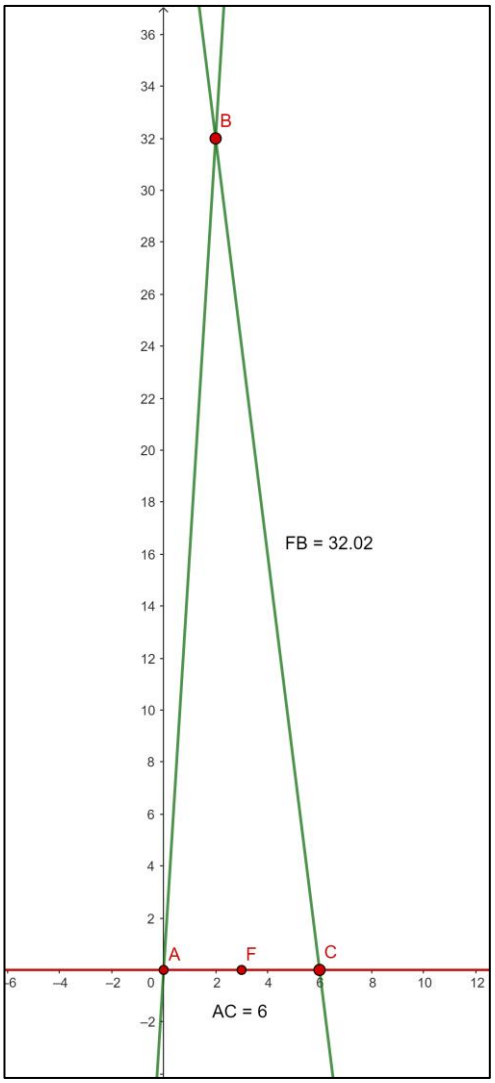


Figure 23: Tall block

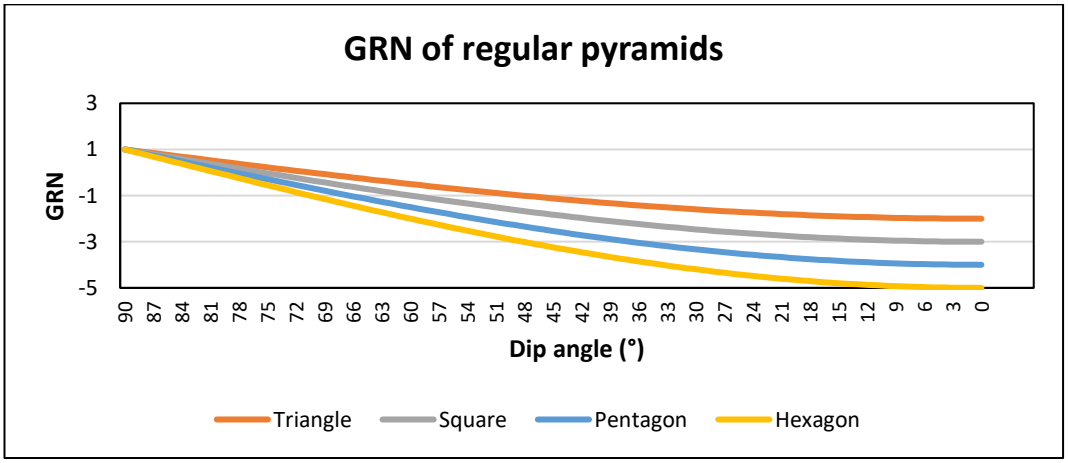


Figure 24: GRN of regular pyramids

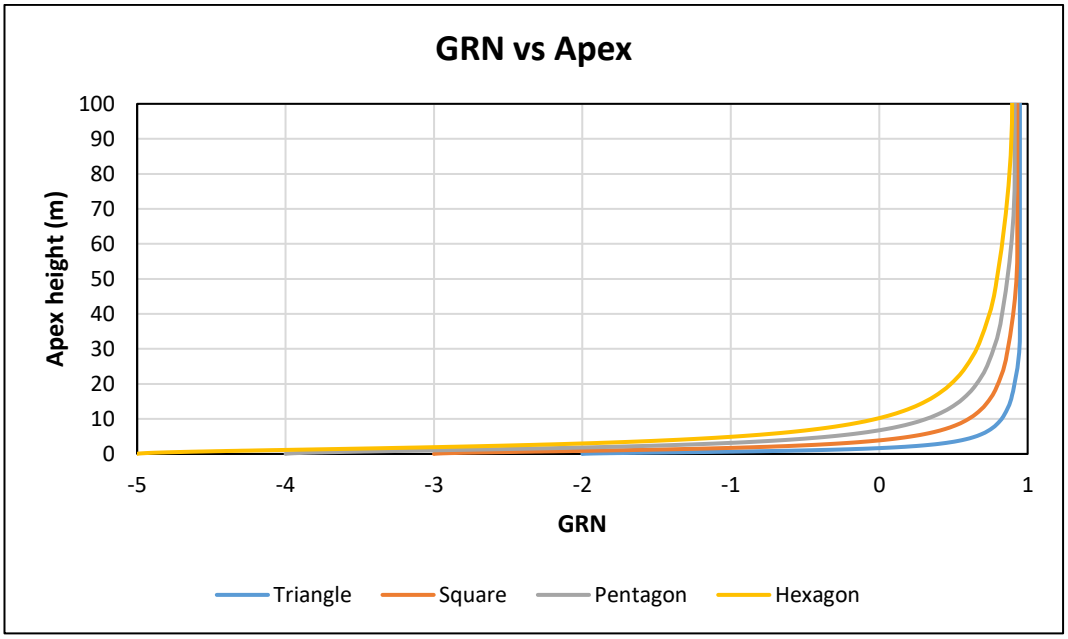


Figure 25: GRN versus apex height

The primary aim of the proposed method is to determine block removability with minimum complexity. The "slenderness" effect, although demonstrated by the GRN, is not within the scope of this research and will not be explored further in this research. A more robust measure of conservancy is required to ensure that a removable block is not classified as non-removable in practice. A fictitious parting plane parallel to the free surface is introduced to "trim" slender blocks in Equation 13 with its contribution to movement equal to $\mathrm{r_{FS}z}$. Equation *13* then becomes Equation *14*:

$$\mathrm{GRN} = (1 + \mathrm{RC}) - (\mathrm{RG} + \mathrm{r_{FS}z}) \qquad \text{Equation 14}$$

The effect of gravity on a solid body, such as a block, is to pull it vertically downwards. However, when an obstacle is introduced in the gravitational path, such as a constraining joint, the effect of gravity is to increase the

normal load on the constraining surface, effectively clamping a block more firmly to the constraining surface. Although the forces acting on a block are not directly considered, the assumption of rigidity implies that forces will be resolved within the confines of the geometric boundaries of the remnant cavity. Hence, a block will only move if the constraining effect of gravity is overcome. An example is provided in the next section.

6.5 Example

The GRN can be calculated easily by setting up a spreadsheet with a few simple formulae. The example is calculated using the inputs from an example put forth by Goodman and Shi (1985), as shown in Table 3 (Goodman and Shi, 1985, p.49). Figure 26 presents a three-dimensional plot of the planes assuming D=1 from Equation *1*.

Table 3: Example inputs (Goodman and Shi, 1985, p.49)

ID	α	β	½ Space
FS	0	90	U
J1	45	90	L
J2	45	330	L
J3	45	210	L

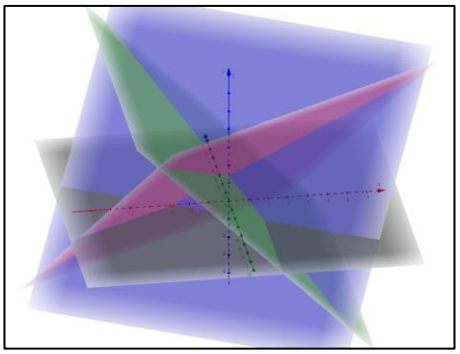


Figure 26: Example planes

The intersection of the planes shown in Figure 26 results in the tetrahedron shown in Figure 27.

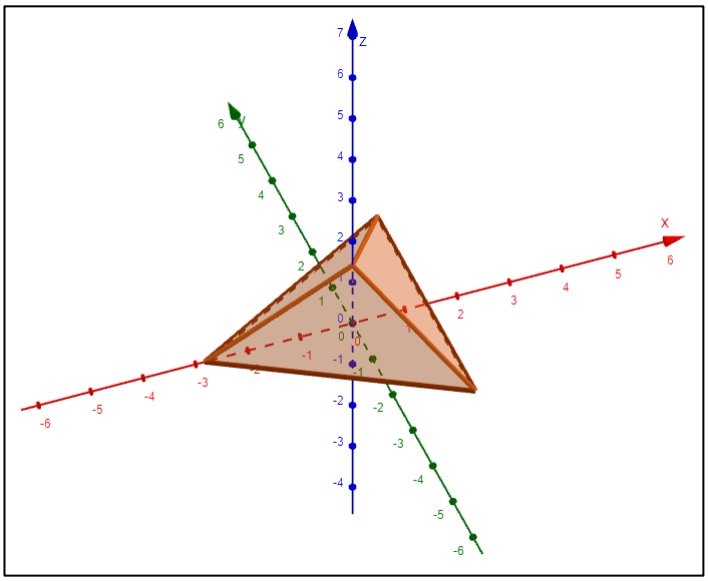


Figure 27: Example tetrahedron

The tetrahedron is determined to be removable according to the GRN as shown in Figure 28.

GRN Calculator												
Input				Upwards unit normal			RMV					
ID	α	β	½ Space	A	B	C	x	y	z	Dot	Contribute	Constrain
FS	0	90	U	0	0	1	0	0	1			
J1	45	90	L	0.707107	4.33E-17	0.707107	0.707107	4.33E-17	0.707107	0.707107	0.7071068	0
J2	45	330	L	-0.35355	0.612372	0.707107	-0.35355	0.612372	0.707107	0.707107	0.7071068	0
J3	45	210	L	-0.35355	-0.61237	0.707107	-0.35355	-0.61237	0.707107	0.707107	0.7071068	0
Removable											2.1213203	0
											GRN	-2.12132

Figure 28: Example 1 GRN calculation

Observed joints underground are typically plotted and extrapolated on mine plans as shown in Figure 29. The simplicity of the GRN method is demonstrated by repeating the example by inspection only.

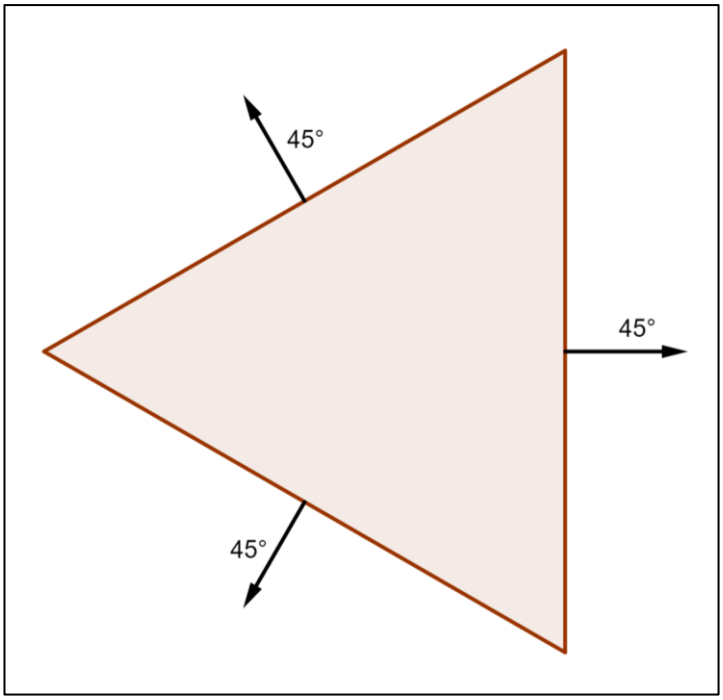


Figure 29: Two-dimensional projection of example tetrahedron

The dip directions are pointing away from the centre of the block; hence the dip directions are also the RMV of each joint. All the joints contribute to block movement, hence the GRN will be less than zero, and therefore the block is removable.

6.6 Chapter Discussion

The research hypothesis was theoretically addressed in this chapter. The rationale leading up to the proposed method was discussed and the base assumptions were described. The mathematical construction of the proposed method was achieved by considering four lemmas and the Gravitational Removability Theorem was formally stated. An example of the application of the theorem was presented. The experimental design is detailed in the next section.

7 EXPERIMENTAL DESIGN

7.1 Chapter Introduction

The gravitational removability theorem was formulated and discussed in the previous chapter. The necessity to test field data is secondary to determining the efficacy of the theorem as field data introduces additional variables, such as roughness and cohesion, which may skew the results. To establish the gravitational removability theorem as a viable method it is necessary to compare the results obtained from the application of the theorem to results on the same data set using an established method. The EV method originally described by Goodman and Shi (1985) as cited by Yan et al. (2023) and briefly discussed in section 5.2 will be used as the comparative base method (Goodman and Shi, 1985; Yan et al., 2023). The reason for choosing the EV method is for computational efficiency. This chapter details the construction of the model to generate the required synthetic data for comparative purposes.

7.2 Block Geometry

To reliably generate synthetic blocks, the geometrical construction of each block must be rigorously defined. Blocks formed by three, four and five constituent joints will be generated to ensure that a sufficiently large range of possible blocks are considered.

The base design of the block generation model involves defining fixed pivot points for each constituent joint. These fixed pivot points are located at the vertices of a triangle, square and pentagon as shown in Figure 30. These

regular polygons are the base centroidal shapes for each set of constituent joints.

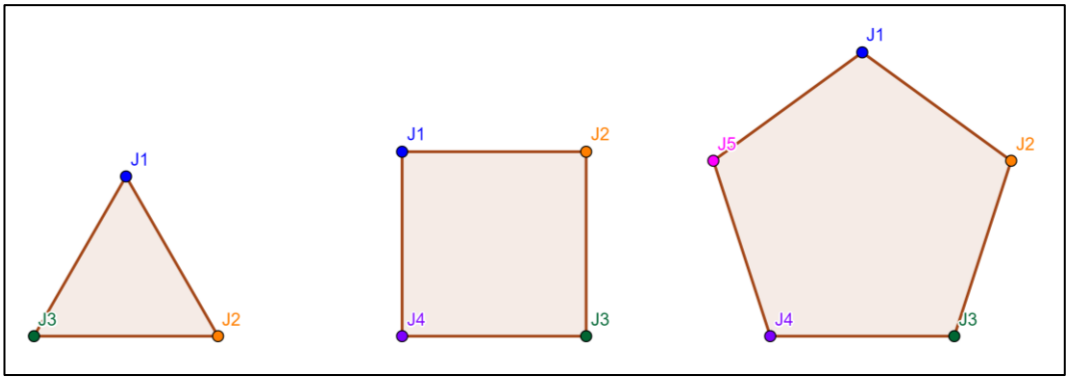


Figure 30: Joint fixed pivot points

The dip direction of each joint must be limited to a specific range to ensure that the number of sides of each block is maintained for each realisation. The scenario may arise where two joints are parallel, or close to parallel which results in a block being either irrationally shaped or the resultant block lying outside of the central shape. This effect is especially detrimental when the number of vertices is odd. A general constraint is applied which does not allow any joint to be rotated closer than 5° from any edge to a base shape.

The constructions for three, four and five joints are shown in Figure 31, Figure 32 and Figure 33 respectively. The dip direction ranges for three, four and five joints are tabulated in Table 4, Table 5 and Table 6 respectively.

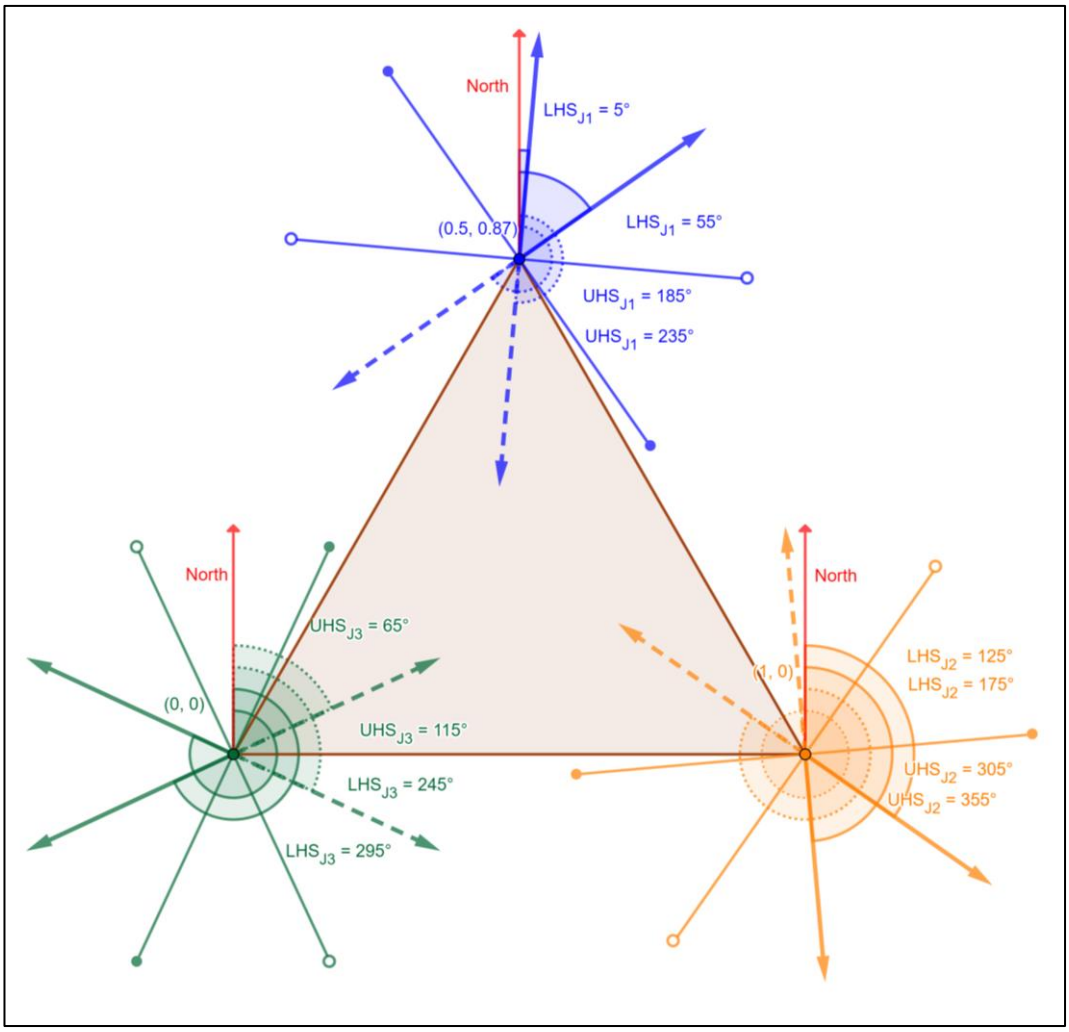


Figure 31: Three-sided limit construction

Table 4: Three-sided block joint dip direction ranges

Joint	LHS range	UHS range	Pivot
J1	5° ≤ 55°	185° ≤ 235°	(0.5, 0.87)
J2	125° ≤ 175°	305° ≤ 355°	(1, 0)
J3	245° ≤ 295°	65° ≤ 115°	(0, 0)

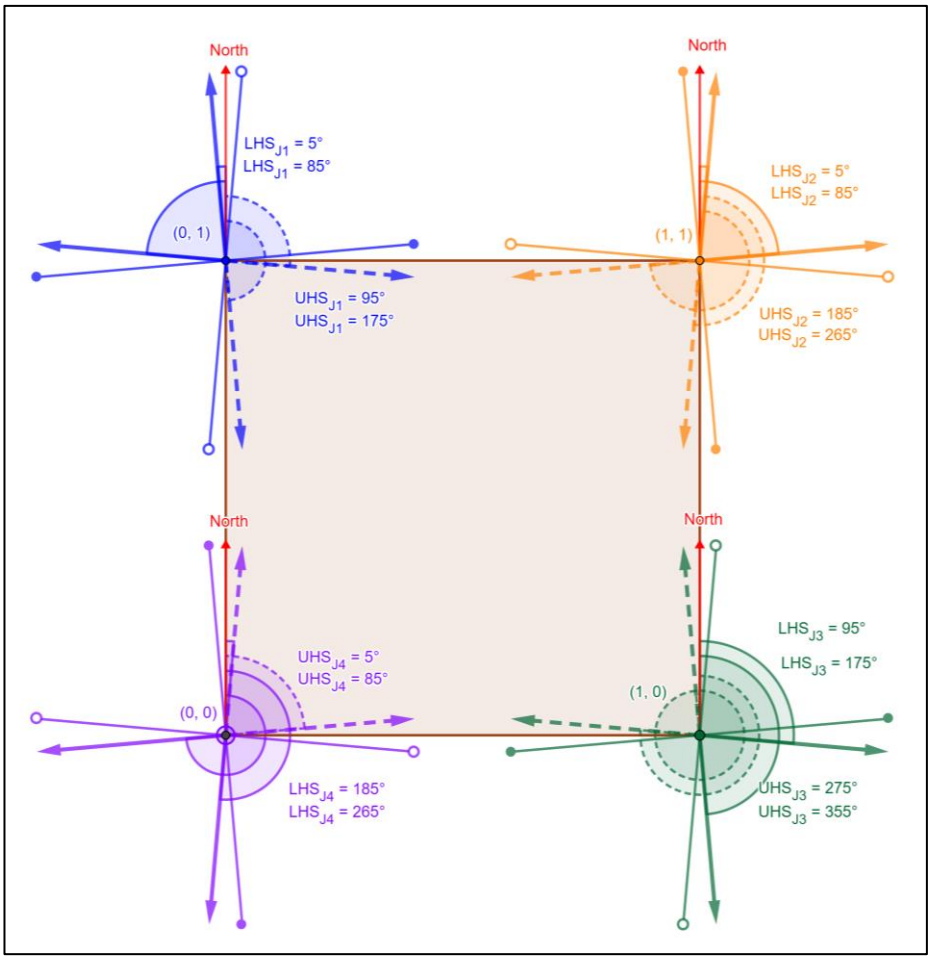


Figure 32: Four-sided limit construction

Table 5: Four-sided block joint dip direction ranges

Joint	LHS range	UHS range	Pivot
J1	-85° ≤ -5°	95° ≤ 175°	(0,1)
J2	5° ≤ 85°	185° ≤ 265°	(1,1)
J3	95° ≤ 175°	275° ≤ 355°	(1, 0)
J4	185° ≤ 265°	5° ≤ 85°	(0,0)

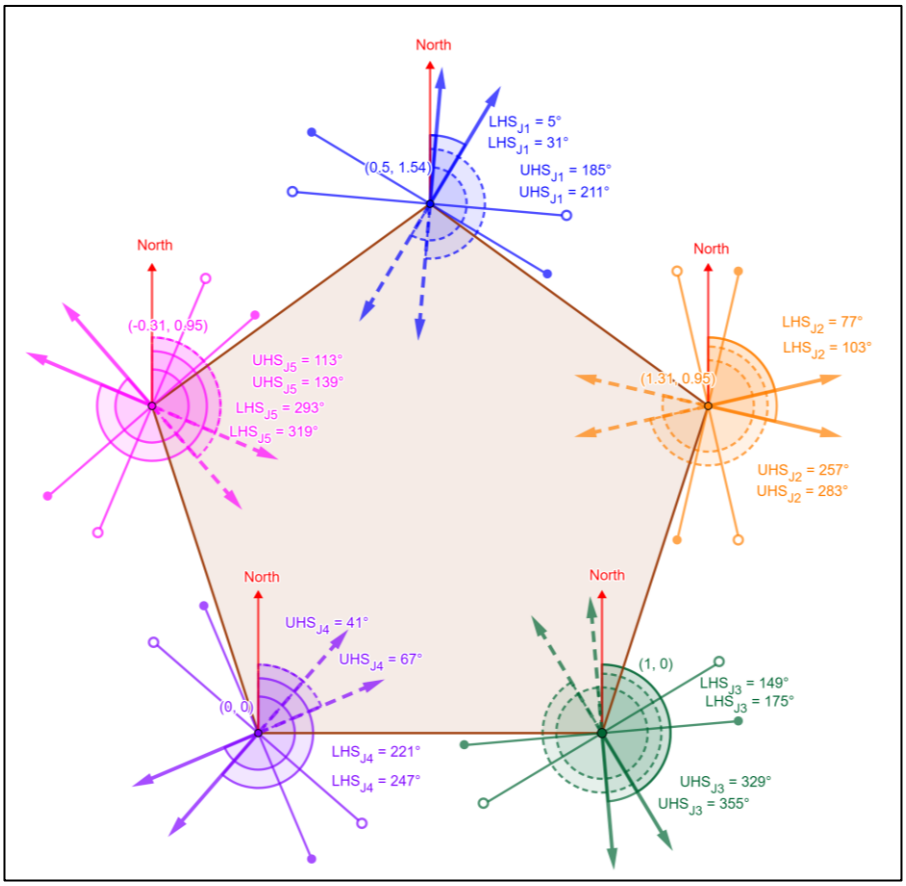


Figure 33: Five-sided limit construction

Table 6: Five-sided block joint dip direction ranges

Joint	LHS range	UHS range	Pivot
J1	5° ≤ 31°	185° ≤ 211°	(0.5, 1.54)
J2	77° ≤ 103°	257° ≤ 283°	(1.31, 0.95)
J3	149° ≤ 175°	329° ≤ 355°	(1, 0)
J4	221° ≤ 247°	41° ≤ 67°	(0, 0)
J5	293° ≤ 319°	113° ≤ 139°	(-0.31, 0.95)

7.3 Edge Vector Method

The EV method was briefly discussed in section 5.2. The method is mathematically detailed here for completeness.

Consider a tetrahedron formed by three joints with planar equations J1, J2 and J3 shifted through the cartesian origin as shown in Equation *15*:

$$\begin{aligned} A_{J1}x + B_{J1}y + C_{J1}z = 0 \\ A_{J2}x + B_{J2}y + C_{J2}z = 0 \\ A_{J3}x + B_{J3}y + C_{J3}z = 0 \end{aligned}$$ Equation 15

The normal upward unit vector for each plane is shown in Equation *16*:

$$\begin{aligned} \hat{n}_{J1} &= (A_{J1}, B_{J1}, C_{J1}) \\ \hat{n}_{J2} &= (A_{J2}, B_{J2}, C_{J2}) \\ \hat{n}_{J3} &= (A_{J3}, B_{J3}, C_{J3}) \end{aligned}$$ Equation 16

If the block is formed in the lower half-spaces of the planes the inwards normal vectors $\hat{I}_{J1}$, $\hat{I}_{J2}$ and $\hat{I}_{J2}$ are given by Equation *17*:

$$\begin{aligned} \hat{I}_{J1} &= -(A_{J1}, B_{J1}, C_{J1}) \\ \hat{I}_{J2} &= -(A_{J2}, B_{J2}, C_{J2}) \\ \hat{I}_{J3} &= -(A_{J3}, B_{J3}, C_{J3}) \end{aligned}$$ Equation 17

The intersection vector between each pair of planes is determined by the cross product of the pair. The cross product between J1 and J2 is shown in Equation *18*:

$$\mathrm{I_{J1J2}} = \hat{\mathrm{I}}_{\mathrm{J1}} \times \hat{\mathrm{I}}_{\mathrm{J2}}$$

$$\mathrm{I_{J1J2}} = \begin{vmatrix} \hat{\imath} & \hat{\jmath} & \hat{k} \\ \mathrm{A_{J1}} & \mathrm{B_{J1}} & \mathrm{C_{J1}} \\ \mathrm{A_{J2}} & \mathrm{B_{J2}} & \mathrm{C_{J2}} \end{vmatrix}$$

$$\mathrm{I_{J1J2}} = \begin{vmatrix} \mathrm{B_{J1}} & \mathrm{C_{J1}} \\ \mathrm{B_{J2}} & \mathrm{C_{J2}} \end{vmatrix} \hat{\imath} - \begin{vmatrix} \mathrm{A_{J1}} & \mathrm{C_{J1}} \\ \mathrm{A_{J2}} & \mathrm{C_{J2}} \end{vmatrix} \hat{\jmath} + \begin{vmatrix} \mathrm{A_{J1}} & \mathrm{B_{J1}} \\ \mathrm{A_{J2}} & \mathrm{B_{J2}} \end{vmatrix} \hat{k}$$

$$\mathrm{I_{J1J2}} = (\mathrm{B_{J1}C_{J2}} - \mathrm{C_{J1B_{J2}}}, \mathrm{C_{J1}A_{J2}} - \mathrm{A_{J1}C_{J2}}, \mathrm{A_{J1}B_{J2}} - \mathrm{B_{J1A_{J2}}})$$

Equation 18

The intersection vector has two directions, the chosen direction must be towards the free surface. When considering the hanging wall this will typically be the intersection vector with a negative z-component.

Once the intersection vectors are determined the scalar product, as detailed in Equation *10*, between the inwards normal unit vector of each plane and each intersection vector is determined. The nine scalar products are shown in Equation *19*.

$$\begin{matrix} \hat{\mathrm{I}}_{\mathrm{J1}}.\mathrm{I_{J1J2}} & \hat{\mathrm{I}}_{\mathrm{J1}}.\mathrm{I_{J2J3}} & \hat{\mathrm{I}}_{\mathrm{J1}}.\mathrm{I_{J1J3}} \\ \hat{\mathrm{I}}_{\mathrm{J2}}.\mathrm{I_{J1J2}} & \hat{\mathrm{I}}_{\mathrm{J2}}.\mathrm{I_{J2J3}} & \hat{\mathrm{I}}_{\mathrm{J2}}.\mathrm{I_{J1J3}} \\ \hat{\mathrm{I}}_{\mathrm{J3}}.\mathrm{I_{J1J2}} & \hat{\mathrm{I}}_{\mathrm{J3}}.\mathrm{I_{J2J3}} & \hat{\mathrm{I}}_{\mathrm{J3}}.\mathrm{I_{J1J3}} \end{matrix}$$

Equation 19

If any of the scalar products is less than zero the block is not removable (Warburton, 1981; Goodman and Shi, 1985; Yan et al., 2023).

7.4 Data Generation Model

Three variables define each joint namely dip, dip direction and half-space. The range of dip angles is arbitrarily chosen to be between 20° and 89°, which is a fair representation of dip angles observed underground. The

Degrees of Freedom (DOF) in terms of the dip direction for each joint are dependent on the base shape and set range as shown in Table 7.

Table 7: Dip direction degrees of freedom

Number of sides	DOF
3	50
4	80
5	26

Assuming only integer values are chosen for the dip and dip direction, the number of possible joints and subsequent shape combinations are shown in Table 8. The sheer number of combinations renders analyses of each possible combination near impossible. Therefore, a data set for each shape will be generated using the Monte Carlo principle, first described by Metropolis and Ulam (1949) (Metropolis and Ulam, 1949). As a baseline 100 000 blocks of each shape will be generated.

Table 8: Possible combinations

Sides	α Range	β Range	½ Space	Joints	Combinations
3	69	50	2	6900	5.47×10^{10}
4	69	80	2	11040	6.19×10^{14}
5	69	26	2	3588	4.94×10^{15}

A spreadsheet will be constructed for each shape considered. The pivot vertices and angular ranges for both the dip and dip direction of each joint are inputs. The free surface is assumed to be a horizontal plane through the cartesian origin. The dip, dip direction and half-space will be randomly selected for each joint for each realisation and the block removability determined using both the EV and GRN methods. A “rinse and repeat” code will record the data from each realisation on a separate data sheet for further analyses.

7.5 Chapter Discussion

The construction of blocks with three, four and five sides was discussed in this chapter. A detailed description of the edge vector method was given, and the construction of the data generator was discussed.

8 RESULTS

8.1 Chapter Introduction

Three data sets were generated according to the experimental design discussed previously. The results and subsequent analyses will be presented in this chapter. A chapter discussion is not presented at the end of this chapter as the complete discussion is presented in the next chapter.

8.2 Data Quality

The half space, dip and dip direction values were randomly generated with every realisation for each joint, which was the primary input into the block generator. Primary analyses cannot continue until the generated data is validated. The purpose of the data quality assessment is to confirm that the generated results are within the specified ranges. In this section, the individual joints are considered as well as the intersection between joints, not the performance of the proposed method. The resulting graphs and figures are provided in Appendices A, B and C.

The following checks were performed on the three data sets:

- Dip angle histogram;
- Dip direction histogram;
- Half-space distribution plot; and
- Inter-joint intersection points.

The range of dip angles for all joints was set between 20° and 89°. The set range was maintained in all the data sets with no outliers. The flatter dip

angles appeared less frequently than the steeper dip angles although several thousand joints were generated with dip angles less than 25°. The histograms for three-sided, four-sided and five-sided blocks are presented in Figure A - 1, Figure B - 1, and Figure C - 1 respectively.

Two ranges of dip direction were specified for each joint according to the half-space of the joint in which each block lies. These ranges were presented in Table 4, Table 5 and Table 6. The set ranges were well maintained as shown in Figure A - 2, Figure B - 2 and Figure C - 2.

The half-space containing each block was randomly selected for each joint during every realisation. The distribution between upper and lower half spaces was fairly even for each joint for all three shapes considered as shown in Figure A - 3, Figure B - 3 and Figure C - 3.

The two-dimensional intersection coordinates between every pair of joints were calculated during every realisation. The number of intersection coordinates for three-sided, four-sided, and five-sided blocks were 300 000, 400 000 and 500 000 respectively.

To present the data meaningfully polygons were plotted using the coordinates corresponding to the minimum and maximum x and y coordinates. The polygon for each pair of joints represents the region where all intersections occurred. In addition, polygons were plotted using the mean intersection coordinates of each joint pair that represent the mean shape.

The base shape was well maintained for each of the three shapes considered. The amount of variation in the two-dimensional footprint can be interpreted as the distance of the intersection polygon vertices from the corresponding mean base shape. The largest ranges of block footprints were achieved by four-sided blocks, followed by three-sided blocks. Five-sided blocks had the smallest range, although the five-sided blocks had the most complex three-dimensional geometries. The intersection range and mean base shapes are presented in Figure A - 4, Figure B - 4 and Figure C - 4.

Three-dimensional examples of a non-removable block for three-sided, four-sided and five-sided two-dimensional footprints are presented in Figure A - 5, Figure B - 5 and Figure C - 5. Similarly, examples of removable blocks are presented in Figure A - 6, Figure B - 6 and Figure C - 6.

8.3 Base Results

In this section, the base statistics and initial comparative results are presented. The removability results calculated using the EV method will be used as the baseline for comparative purposes throughout. The base statistics and a base comparison are presented in Table 9.

Table 9: Base comparison

Base Comparison			
Number of constituent joints	**3**	**4**	**5**
Base Statistics			
Blocks generated	100,000	100,000	100,000
Removable according to EV	47,417	15,988	4,184
Non-removable according to EV	52,583	84,012	95,816
EV & GRN removable			
Count	42,789	15,480	4,179
Agreement	90%	97%	99.88%
% of total blocks	43%	15%	4%
EV & GRN non-removable			
Count	45,332	49,405	49,927
Agreement	86%	59%	52%
% of total blocks	45%	49%	50%
EV removable / GRN non-removable			
Count	4,628	508	5
Disagreement	10%	3%	0.12%
% of total blocks	5%	1%	0%
EV non-removable / GRN removable			
Count	7,251	34,607	45,889
Disagreement	14%	41%	48%
% of total blocks	7%	35%	46%

8.4 Calibrated Results

The calibrated results following the application of geometric conditions are presented in Table 10.

Table 10: Calibrated balance sheet

Calibrated Balance Sheet					
Number of constituent joints			**3**	**4**	**5**
Number of blocks generated			**100,000**	**100,000**	**100,000**
Geometric calibration					
1.	Outright removable	All LHS	(633)	(1,554)	(1,558)
2.	Opposite constrained	UHS-UHS	0	(7,112)	(18,834)
3.	Constrained by collision	α-UHS < α-LHS	0	(17,430)	(20,236)
4.	Potential rotation	At least 1 UHS	(11,246)	(9,019)	(5,266)
Subtotal			**88,121**	**64,885**	**54,106**
EV & GRN removable			(42,789)	(15,480)	(4,179)
EV & GRN non-removable			(45,332)	(49,405)	(49,927)
Blocks not accounted			**0**	**0**	**0**

8.5 Potential Rotation

The geometric conditions from one to three shown in Table 10 yields a direct binary decision in terms of removability but the fourth condition still presents a measure of uncertainty. The calculated values of the GRN for those blocks classified as potentially rotational were analysed further to understand this uncertainty.

A plot of the GRN values for three-sided blocks where the EV method implies removability and the GRN not is shown in Figure 34.

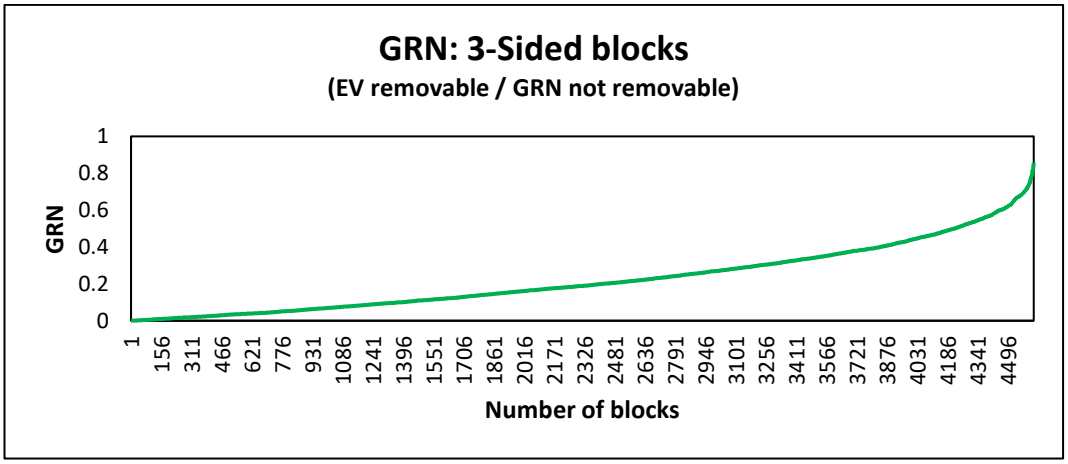


Figure 34: 3-Sided plot of GRN (EV removable / GRN not removable)

A plot of the GRN values for three-sided, four-sided, and five-sided blocks where the EV method implies non-removability and the GRN implies removability is shown in Figure 35.

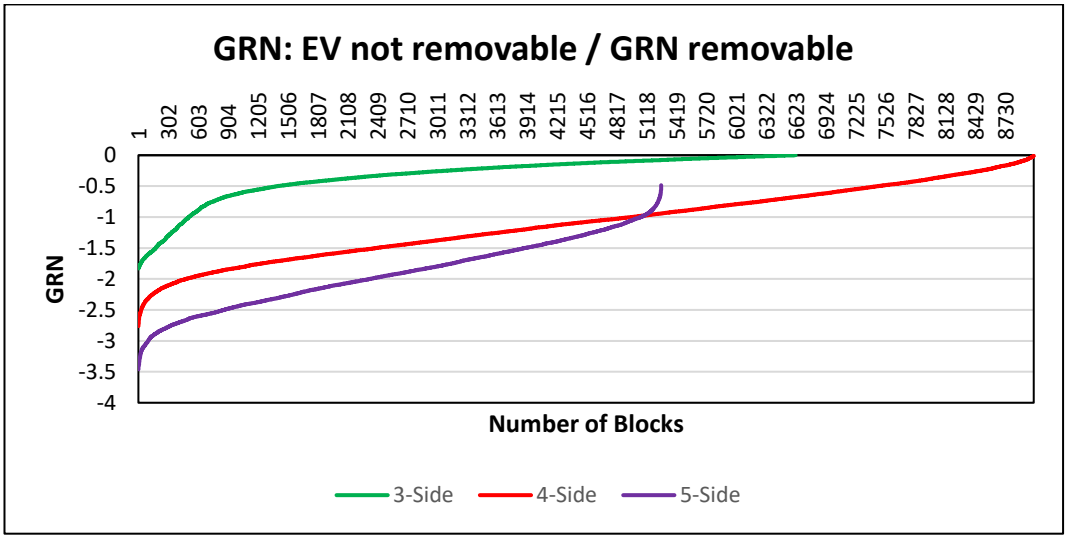


Figure 35: GRN removable / EV not removable

9 DISCUSSION

The primary data for this research project was obtained from the output of a block generation model, which was constructed for this purpose. The block generator consists of several spreadsheets and computer code written in Visual Basic for Applications (VBA). The principal variables that govern block geometry are the dip angle, dip direction angle and the half space in which the block lies.

The Monte Carlo approach was applied to generate the blocks by randomly varying the three primary variables within set ranges. The two general steps when conducting Monte Carlo analyses are producing many pseudo-random input values of variables within a range applicable to each variable and then using the values deterministically (Metropolis and Ulam, 1949). Following this approach 100 000 realisations were done for blocks formed by three, four and five joints, resulting in a total of 300 000 blocks formed by a total of 1 200 000 joints. The conformity of the generated data was assessed in section 8.2 and found to be satisfactory.

An initial direct comparison was made between the EV and GRN methods in section 8.3. A balanced representation was achieved for three-sided and four-sided blocks, but the five-sided blocks are strongly skewed towards non-removability. This phenomenon is expected since block removability decreases with increased geometric complexity. The GRN agrees strongly with the EV method with agreement in the 90 percentiles for all base shapes,

in terms of removability as geometric complexity increases. Direct agreement in terms of non-removability is poorer, although when considering that the primary disparity lies in the GRN overstating removability, it can be regarded as a conservancy factor. This effect is caused by the inclusion of a fictitious parting plane in the GRN calculation; hence the conservancy is expected.

The highest risk is incurred by classifying a block as non-removable when it is, in fact, removable, which may lead to dangerously wrong decisions. Although the highest occurrence of this phenomenon is 5%, which corresponds to a probability of 0.05, the discrepancy needs further investigation.

The disregard for the physical geometry of a block by the GRN implies that certain geometric conditions may lead to the misclassification of blocks in its application. GRN assumes that geometrically constrained blocks are discarded outright before calculation. The fictitious parting plane included in the GRN may also lead to misclassification, especially in instances where the joint dips are steeper, resulting in lower z-components, which may be insufficient to overcome the contribution of the fictitious plane.

The effect of opposing constraints on four-sided blocks was discussed in section 6.2. A four-sided block can be classified outright as non-removable under the following conditions, which are graphically represented in Figure 36:

- A block lies in the UHS of all the constituent joints;
- A block lies in the UHS of two opposing joints; and
- A block lying in the UHS of a joint and in the LHS of the opposing joint where the dip angle of the upper half space joint is lower than that of the opposing joint.

When a block lies in the LHS of all the constituent joints the block is outright removable as shown in Figure 37.

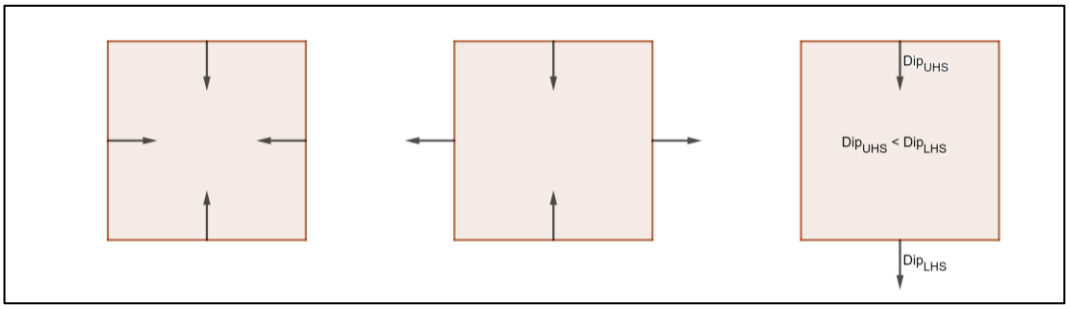


Figure 36: Four-sided non-removable conditions

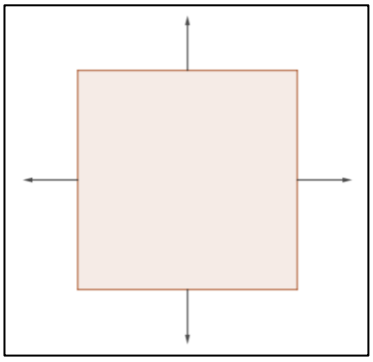


Figure 37: Outright removable four-sided block

The rationale discussed for four-sided blocks was applied to both the three-sided and the five-sided blocks with similar results. The balance of the

disagreement between the EV method and GRN was comprised of blocks formed in the UHS of one constituent joint.

Such a geometry implies that at least one apex of the block lies outside of the two-dimensional footprint of the block on the free surface. Such a block will not necessarily be removable through translation, but rather through rotation, which is not addressed by the edge vector method. An example of such a block is given in Figure 38. It is concluded that when a block is formed where it lies in the upper half space of at least one constituent joint the block can be potentially removable through rotation.

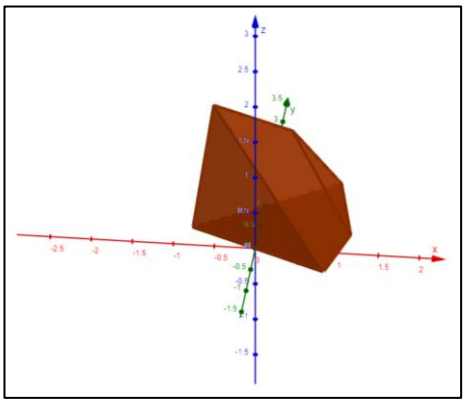


Figure 38: Potential rotationally removable four-sided block

The blocks regarded as potentially removable through rotation were further analysed in section 8.5. The scenario where the EV method implies removability and the GRN not yielded 4,628 data points for three-sided blocks, two for four-sided blocks and none for five-sided blocks. The inverse scenario where EV method implies non-removability and the GRN implies removability was significantly more prevalent.

The GRN values when considering the first scenario were all equal to or greater than zero. The GRN values when considering the second scenario were all less than zero. This clear distinction in the data leads to the conclusion that a block that lies in the upper half space of at least one constituent joint and remains unclassified following the application of the geometric filters is removable when the GRN is greater than zero. Conversely, if the GRN is less than or equal to zero the block is removable by rotation.

10 CONCLUSION

The gap identified in the existing body of knowledge is that the routine application of KBT is limited due to the computational complexity involved. The primary objective of this research project was to devise a method to determine block removability that requires minimal if any, calculation to make KBT routinely available to the miner. Determining block removability is more important than stability analysis in the context of day-to-day mining. A colloquial view is that *"If it can move, it can fall"*, which is an accurate statement considering daily underground mining. The research hypothesis to address the gap is:

The removability of a convex block, defined by a free surface and several discontinuities, can be judged by considering only the summation of the components of the normal vectors of the constituent joints pointing away from the centroid of the block, relative to the gravitational vector where the contribution of any joint to removability is relative to angle between the normal vector of the free surface pointing into the rock mass and the normal vector of the joint pointing away from the centroid of the block.

A hypothetical model was constructed to satisfy the research hypothesis. The vector normal to a plane in the direction of the rock mass is central to the hypothetical model and was determined through the application of Lemma 1 and Lemma 2. The contribution of a joint to the overall block removability was determined through the application of Lemma 3 and

Lemma 4. Equation *14* was newly formulated to calculate the gravitational removability number. The gravitational removability theorem was formally stated as:

A block formed by the intersection of a free surface and several joints is not removable when its gravitational removability number is greater than zero. A block is removable when its gravitational removability number is less than zero.

The data analysis, however, revealed a strong correlation in terms of removable blocks but the correlation with regards to non-removable blocks was unsatisfactory. Analyses revealed that the source of the misclassification was the disregard for physical geometry in the calculation of the gravitational removability number. The instances where disparity existed between the results obtained by the EV method and the GRN method did provide valuable insights which led to the definition of a set of geometric conditions. These geometric conditions allow for blocks to be regarded as removable or not outright by inspection of a block's two-dimensional footprint and dip direction vectors only. Joints are typically indicated as lines, with arrows indicating dip directions on mine plans. The significance is that any mine worker, even illiterate, can, with minimal training, identify potentially dangerous blocks by simply looking at a mine plan.

Application of the geometric conditions on the data set addressed all disparities between the EV method and the GRN method. In addition, a comparison of the actual GRN with the EV results in the disparate cases revealed that the GRN, when considered in conjunction with the geometric conditions, can indicate rotational removability, whereas the EV method only considers translational removability.

Three significant outcomes were achieved through this research:

- Data analyses provided sufficient evidence that the hypothesis is accepted within the confines of the stated assumptions;
- A set of geometric conditions was developed that allows any mine worker to identify potentially removable blocks from a mine plan without any calculation; and
- Application of the gravitational removability number in conjunction with the geometric conditions reveals blocks potentially removable through rotation, a mechanism not addressed by the edge vector method.

In conclusion, the application of the geometric conditions and GRN enables the determination of block removability with no or minimal need for calculation. The primary objective of this research project was achieved.

11 RECOMMENDATIONS

The following recommendations for further research are made:

- There appears to be a relationship between the GRN and block apex height, which may potentially lead to significant insights;
- The GRN was only considered as being positive or negative, the actual value of the GRN was not interrogated further. Assigning meaning to the actual number may lead to interesting results; and
- The development and implementation of a TARP system based on the gravitational removability theorem and its effect on overall FOG occurrences and related injuries will be very significant.

REFERENCE LIST

Azarafza, M. and Zhu, H.H., 2022. *Key-block theorem application on discontinuous rock slope instabilities and rock mass description.* In: *Lecture Notes in Civil Engineering*. Springer Science and Business Media Deutschland GmbH. pp.200–208. https://doi.org/10.1007/978-981-16-9963-4_16.

Baecher, G., 1983. *Statistical analysis of rock mass fracturing*. Journal of the International Association for Mathematical Geology, 15, pp.329–348. https://doi.org/10.1007/BF01036074.

Baecher, G., and Lanney, N.A., 1978. *Trace length biases in joint surveys*. 19th U.S. Symposium on Rock Mechanics, 1, pp.56–65.

Barton, N., Lien, R. and Lunde, J., 1974. *Engineering classification of rock masses for the design of tunnel support*. Rock mechanics, [online] 6(4), pp. 189–236. https://doi.org/10.1007/BF01239496.

Bernaix, J., 1967. *Etude géotechnique de la roche de Malpasset*.

Bieniawski, Z.T., 1973*. Engineering classification of jointed rock masses*. The civil engineer in South Africa, pp. 335–343.

Blahůt, J. and Racek, O., 2023. *Modern methods of rock mass characterisation and rockfall monitoring: a review*. In: Landslides:

Detection, Prediction and Monitoring. [online] Cham: Springer International Publishing. pp. 1–38. https://doi.org/10.1007/978-3-031-23859-8_1.

Brown, E.T., 2007. *Block Caving Geomechanics: International Caving Study 1997-2004*. Julius Kruttschnitt Mineral Research Centre, The University of Queensland.

Call, R.D., 1972. *Analysis of geologic structure for open pit slope design*. University of Arizona.

Call, R.D., Savely, J.P. and Nicholas, D., 1976. *Estimation of joint set characteristics from surface mapping data.* [online] Available at: <https://api.semanticscholar.org/CorpusID:126942832>.

Chen, J.P., Lu, B., Wang, L.K. and Li, X.C., 2003. *Automatic search for complex unstable rock block and the judgment of unstability mode-based on 3D network simulation of random fractures*. Chinese Journal of Rock Mechanics and Engineering, 22(7), pp. 1126–1131.

Chen, Q., Qin, S., Yin, T. and Zhen, W., 2019. *Search and graphical display of hazardous blocks in underground roadway roofs*. International Journal of Rock Mechanics and Mining Sciences, [online] 123 (104095) https://doi.org/10.1016/j.ijrmms.2019.104095.

Cheng, X.L., Liu, L.P., Xiao, J., Zhang, Q.H., Jiao, Y.Y., Zheng, F. and Wang, Y., 2021a. *Analysing block stability under varying resultant force for arbitrary shapes.* IOP Conference Series: Earth and Environmental Science, [online] 861(3), 32062. https://doi.org/10.1088/1755-1315/861/3/032062.

Cheng, X.L., Liu, L.P., Xiao, J., Zhang, Q.H., Xue, J. and Wang, Y., 2021b. *A general block stability analysis algorithm for arbitrary block shapes*. Frontiers in Earth Science, 9. https://doi.org/10.3389/feart.2021.723320.

Chikande, T. and Zvarivadza, T., 2018. *Evaluation of tendon support in anisotropic jointed rockmass.* In: ARMA US Rock Mechanics/Geomechanics Symposium. ARMA. 2018.

Cook, J.B., Libby, J.W. and Madil, j. T., 1962. *Kemano tunnel, operation and maintenance.* The Engineering Journal, 45, pp. 39–86.

Cormen, T.H., Leiserson, C.E., Rivest, R.L. and Stein, C., 2009. *Introduction to Algorithm, the third edition*. In: USA, MIT Press.

Cruden, D.M., 1977. *Describing the size of discontinuities*. International Journal of Rock Mechanics and Mining Sciences & Geomechanics Abstracts, [online] 14(3), pp. 133–137. https://doi.org/10.1016/0148-9062(77)90004-3.

Dunn, M.J., Hagan, P. and Saydam, S., 2010. *The application of probabilistic keyblock methods for support design in blocky rock masses*. In: Proceedings 2nd Australasian Ground Control in Mining Conference, P. Hagan and S. Saydam (eds). pp. 23–24.

Dunn, M.J. and Stacey, T.R., 2008. *Design of stable spans at Tau Lekoa Mine.* In: SHIRMS 2008: Proceedings of the First Southern Hemisphere International Rock Mechanics Symposium. Australian Centre for Geomechanics. pp. 179–192.

Esterhuizen, G.S., 2023a. *Software by GS Esterhuizen - About*. Available at: <https://sites.google.com/view/ayzprojects/about>.

Esterhuizen, G.S., 2023b. *Software by GS Esterhuizen - Purchase*. Available at: <https://sites.google.com/view/ayzprojects/about-us>.

Esterhuizen, G. S., and Streuders, S. B. (1998). *Rockfall hazard evaluation using probabilistic keyblock analysis*. The Journal of The South African Institute of Mining and Metallurgy, April, 59–64.

Fernández, A., Sanchidrián, J.A., Segarra, P., Gómez, S., Li, E. and Navarro, R., 2023. *Rock mass structural recognition from drill monitoring technology in underground mining using discontinuity index and machine learning techniques*. International Journal of

Mining Science and Technology, [online] 33(5), pp. 555–571. https://doi.org/10.1016/j.ijmst.2023.02.004.

Ferrero, A.M., Segalini, A. and Giani, G.P., 2010. *Stability analysis of historic underground quarries*. Computers and Geotechnics, 37(4), pp. 476–486. https://doi.org/10.1016/j.compgeo.2010.01.007.

Gardner, L. J., Bronkhorst, L., and N. L. Ayres. *Optimizing Stope Panel Spans at an Eastern Bushveld Platinum Mine by Probabilistic Analysis.* Paper presented at the ISRM AfriRock - Rock Mechanics for Africa, Cape Town, South Africa, October 2017.

Geo&soft, 2006. User guide ROCK3D three-dimensional rock block analysis based key block theory ROCK3D-user guide.

Geo&Soft, 2023. Order. [online] Available at: <https://www.geoandsoft.com/english/order.htm>.

Ghazal, R., 2013. *Stability modeling of isolated rock blocks at the surface of underground excavations taking into account initial stresses and non-linear joint behavior*. PhD. Ecole Nationale Supérieure des Mines de Paris.

Ghazal, R., Hadj Hassen, F. and Tijani, M., 2011. *A new numerical model to study isolated rock blocks around underground excavations*

taking into account in-situ stresses. 45th US Rock Mechanics / Geomechanics Symposium.

Ghazal, R., Hadj Hassen, F. and Tijani, M., 2012. *Stability modelling of isolated rock blocks at the surface of underground excavations taking into account in-situ stresses.* Harmonising Rock Engineering and the Environment - Proceedings of the 12th ISRM International Congress on Rock Mechanics, pp. 391–394. https://doi.org/10.1201/b11646-66.

Goodman, R. E. and Shi, G. 1985. *Block Theory and Its Application to Rock Engineering*. Englewood Cliffs N.J: Prentice-Hall.

Goodman, R.E., Taylor, R.L. and Brekke, T.L., 1968. *A Model for the Mechanics of Jointed Rock*. Journal of the Soil Mechanics and Foundations Division, 94(3), pp. 637–659. https://doi.org/10.1061/JSFEAQ.0001133.

Groundwork Consulting, 2023. M*AR_03665_RES_SSS_Itasca_Software_Quote_Christiaan van Rooyen*. Johannesburg.

Haile, A.T. and Jager, A.J., 1995. *Rock mass condition, behaviour and seismicity in the mines of the Bushveld Igneous Complex*. GAP 027.

Heliot, D., 1988. *Generating a blocky rock mass*. International Journal of Rock Mechanics and Mining Sciences & Geomechanics Abstracts, [online] 25(3), pp. 127–138. https://doi.org/10.1016/0148-9062(88)92295-4.

Herrero, M.J., Pérez-Fortes, A.P., Escavy, J.I., Insua-Arévalo, J.M., De la Horra, R., López-Acevedo, F. and Trigos, L., 2022. *3D model generated from UAV photogrammetry and semi-automated rock mass characterization*. Computers & Geosciences, [online] 163, 105121. https://doi.org/10.1016/j.cageo.2022.105121.

Hu, J., Yang, C., Zhou, K., Li, J. and Gao, F., 2016. *Stability of undercut space in fragment orebody based on key block theory*. Transactions of Nonferrous Metals Society of China, [online] 26(7), pp. 1946–1954. https://doi.org/https://doi.org/10.1016/S1003-6326(16)64305-4.

International Society for Rock Mechanics (ISRM), 1978. *Suggested Methods for the Quantitative Description of Discontinuities in Rock Masses*. International Journal of Rock Mechanics and Mining Sciences & Geomechanics Abstracts, 15, pp. 319–368.

Joughin, W.C., Jager, A., Nezomba, E. and Rwodzi, L., 2012a. *A risk evaluation model for support design in Bushveld Complex underground mines: Part I-Description of the model*. Journal of the

Southern African Institute of Mining and Metallurgy, 112(2), pp. 83–94.

Joughin, W.C., Jager, A., Nezomba, E. and Rwodzi, L., 2012b. *A risk evaluation model for support design in Bushveld Complex underground mines: Part II-Model validation and case studies*. Journal of the Southern African Institute of Mining and Metallurgy, 112(2), pp. 95–104.

Judeel, G., Swanepoel, T., Holder, A., Swarts, B., Van Strijp, T. and Cloete, A., 2016. *Extension of the Cullinan Diamond Mine No. 1 Shaft underneath the existing operating shaft*. Journal of the Southern African Institute of Mining and Metallurgy, 116(8).

Khoza, K.R., Hingston, E.D.C., Mtshali, S., Khumalo, C. and Mabogo, N., 2019. *The Use of JBlock in the Analysis of Potential Rock Falls at the Magdalena Colliery, Dundee, South Africa*. In: IAEG/AEG Annual Meeting Proceedings, San Francisco, California, 2018- Volume 1: Slope Stability: Case Histories, Landslide Mapping, Emerging Technologies. Springer. pp. 101–109.

Kim, D.H., Gratchev, I. and Balasubramaniam, A., 2015. *Back analysis of a natural jointed rock slope based on the photogrammetry method*. Landslides, [online] 12(1), pp. 147–154. https://doi.org/10.1007/s10346-014-0528-3.

Kulatilake, P.H.S.W. and Wu, T.H., 1984. *Sampling bias on orientation of discontinuities*. Rock Mechanics and Rock Engineering, [online] 17(4), pp. 243–253. https://doi.org/10.1007/BF01032337.

Langenhoven, H., 2023. *Facts & Figures Pocketbook 2022*. Johannesburg.

Li, X., Yao, M., Yuan, J., Wang, Y. and Li, P., 2023. *Deep learning characterization of rock conditions based on tunnel boring machine data*. Underground Space, [online] 12, pp. 89–101. https://doi.org/https://doi.org/10.1016/j.undsp.2022.10.010.

Liu, B., He, K., Han, M., Hu, X., Wu, T., Wu, M. and Ma, G., 2021. *Dynamic process simulation of the Xiaogangjian rockslide occurred in shattered mountain based on 3DEC and DFN*. Computers and Geotechnics, [online] 134,104122. https://doi.org/https://doi.org/10.1016/j.compgeo.2021.104122.

Liu, J., Li, Z. and Zhang, Z., 2004. *Stability analysis of block in the surrounding rock mass of a large underground excavation.* Tunnelling and Underground Space Technology, [online] 19(1), pp. 35–44. https://doi.org/https://doi.org/10.1016/S0886-7798(03)00084-1.

Mathis, J.I., 1988. *Development and verification of a three dimensional rock joint model*. Luleå tekniska universitet.

Metropolis, N. and Ulam, S., 1949. *The monte carlo method*. Journal of the American statistical association, 44(247), pp. 335–341.

Netshilaphala, V. and Zvarivadza, T., 2022. *Fall of ground management through underground joint mapping: shallow chrome mining case study*. Geotechnical and Geological Engineering, 40(4), pp. 2231–2254.

Nezomba, E., 2012. *Use of joint trace data to evaluate stability of mining excavations, and validation against underground observations*. University of the Witwatersrand.

Noroozi, M., Jalali, S.E. and Yarahmadi-Bafghi, A.R., 2012. *3D key-group method for slope stability analysis*. International journal for numerical and analytical methods in geomechanics, 36(16), pp. 1780–1792.

Priest, S.D. and Hudson, J.A., 1981. *Estimation of Discontinuity Spacing and Trace Length Using Scanline Surveys*. International Journal of Rock Mechanics and Mining Sciences & Geomechanics Abstracts, Volume 18, Issue 3,1981, pp. 183-197, ISSN 0148-9062, https://doi.org/10.1016/0148-9062(81)90973-6.

Quang Minh, N., Truong Thanh, P., Manh Tuan, D., Xuan Truong, T., Trung Kien, L., Thi Phuong Thanh, N. and Thi Hong Cam, V., 2020.

A case study along 3B highway, Xuat Hoa area, Bac Kan province. Science on Natural Resources and Environment Journal homepage: tapchikhtnmt.hunre.edu.vn BLOCK THEORY ANALYSES FOR ROCK SLOPE STABILITY.

Rocscience, 2022. *UnWedge - Wedge Calculations, Theory Manual*.

Rocscience, 2023. *UnWedge*.

Rocscience.com, 2013. *Isolated Block Stability Method — 3DEC 7.0 documentation*. Available at: <https://docs.itascacg.com/3dec700/3dec/docproject/source/theory/3dectheory/isolatedblock.html>.

Rocscience.com, 2023. *UnWedge | Stability analysis for underground excavations in rock*. [online] Available at: <https://www.rocscience.com/software/unwedge#pricing>.

Schwab, K., 2016. *The Fourth Industrial Revolution*. [online] Available at: <www.weforum.org>.

Sewnun, D., Joughin, W.C., Armstrong, R. and Cooper, A., 2017. *Keyblock stability analysis of longhole stopes*. Paper presented at the ISRM AfriRock - Rock Mechanics for Africa, Cape Town, South Africa, October 2017.

Terzaghi, R.D., 1965. *Sources of Error in Joint Surveys*. Géotechnique, [online] 15(3), pp. 287–304. https://doi.org/10.1680/geot.1965.15.3.287.

Villaescusa, E., 1992. *A review and analysis of rock discontinuity mapping methods*. [online] Available at: <https://www.researchgate.net/publication/269931290>.

Wang, H., Song, F., Chen, Y., Li, T. and Ma, G., 2023. *Stability analysis of fractured rock masses based on an extended key block theory considering the forces between blocks and block rotation*. Tunnelling and Underground Space Technology, [online] 132, 104895. https://doi.org/https://doi.org/10.1016/j.tust.2022.104895.

Wang, S., Zhang, Z., Huang, X., Huang, Y. and Lei, Q., 2021. *A generalized joint pyramid method for removability analysis of rock blocks: Theoretical formulation and numerical implementation*. Computers and Geotechnics, [online] 132, 103972. https://doi.org/https://doi.org/10.1016/j.compgeo.2020.103972.

Warburton, P.M., 1981. *Vector stability analysis of an arbitrary polyhedral rock block with any number of free faces*. International Journal of Rock Mechanics and Mining Sciences & Geomechanics Abstracts. 1981; 18:415-427. http://hdl.handle.net/102.100.100/291033?index=1.

Wu, F., Wu, J., Bao, H., Bai, Z., Qiao, L., Zhang, F., Li, B., Si, F., Yu, L., Guan, S., Sha, P., Kong, D., Dai, Z., Chen, K., Tian, Y. and Liu, C., 2023. *Rapid intelligent evaluation method and technology for determining engineering rock mass quality*. Rock Mechanics Bulletin, [online] 2(2), 100038. https://doi.org/https://doi.org/10.1016/j.rockmb.2023.100038.

Wu, J.-H., Lin, W.-K. and Hu, H.-T., 2018. *Post-failure simulations of a large slope failure using 3DEC: The Hsien-du-shan slope*. Engineering Geology, [online] 242, pp. 92–107. https://doi.org/https://doi.org/10.1016/j.enggeo.2018.05.018.

Wu, W., Zhuang, X., Zhu, H., Liu, X. and Ma, G., 2017. *Centroid sliding pyramid method for removability and stability analysis of fractured hard rock*. Acta Geotechnica, [online] 12(3), pp. 627–644. https://doi.org/10.1007/s11440-016-0510-4.

Xia, L., Yu, Q., Chen, Y., Li, M., Xue, G. and Chen, D., 2015. *GeneralBlock: A C++ Program for Identifying and Analyzing Rock Blocks Formed by Finite-Sized Fractures*. IFIP Advances in Information and Communication Technology, https://doi.org/10.1007/978-3-319-15994-2_52.

Yan, J., Chen, J., Zhang, Y., Liu, Y., Zhao, X., Xue, J., Zhu, C., Mehmood, Q. and Wang, Q., 2023. *Semi-automatic extraction of dangerous*

rock blocks from jointed rock exposures based on a discontinuity trace map. Computers and Geotechnics, 156. https://doi.org/10.1016/j.compgeo.2023.105265.

Yarahmadi Bafghi, A.R. and Verdel, T., 2003. *The key-group method*. International journal for numerical and analytical methods in geomechanics, 27(6), pp. 495–511.

Yow, J.L., 1985. *Field investigation of keyblock stability*. PhD. University of California.

Yu, Q., Xue, G. and Chen, D., 2007. *General block method of fractured rock mass.* China Waterpower Press.

Yu, Q.-C., Chen, D.-J., Xue, G.-F. and Yuzo, O., 2005. *Preliminary study on general block method of fractured rock mass*. Hydrogeology & Engineering Geology, 32(6), pp. 42–48.

Zerradi, Y., Lahmili, A. and Souissi, M., 2020. *Stability of a rock mass using the key block theory: a case study*. E3S Web Conf., [online] 150. Available at: <https://doi.org/10.1051/e3sconf/202015003024>.

Zerradi, Y., Souissi, M. and Larabi, A., 2023. *Application of the deterministic block theory to the slope stability design of an open-pit mine in Morocco*. Mining of mineral deposits, 17(2), pp. 53–60.

Zerradi, Y., Souissi, M., Soufi, A., Bennouna, R., Bahi, A. and Zaki, I., 2023. *Slope stability assessment using slope mass rating (smr), key block theory, and kinematic analysis: a case study*. Journal of Southwest Jiaotong University, 58(4). https://doi.org/10.35741/issn.0258-2724.58.4.45.

Zhang, L. and Qing-chun, Y.U., 2010. *Theoretical validation on general block method*. Hydrogeology & Engineering Geology, 37(6), pp. 55–60.

Zhang, L., Sherizadeh, T., Zhang, Y., Sunkpal, M., Liu, H. and Yu, Q., 2020. Stability analysis of three-dimensional rock blocks based on general block method. Computers and Geotechnics, [online] 124, p.103621. https://doi.org/https://doi.org/10.1016/j.compgeo.2020.103621.

Zhang, Z. and Kulatilake, P.H.S.W., 2003. *A new stereo-analytical method for determination of removal blocks in discontinuous rock masses*. International journal for numerical and analytical methods in geomechanics, 27(10), pp. 791–811.

Zhao, M., Song, S., Wang, F., Zhu, C., Liu, D. and Wang, S., 2023. *A method to interpret fracture aperture of rock slope using adaptive shape and unmanned aerial vehicle multi-angle nap-of-the-object photogrammetry*. Journal of Rock Mechanics and Geotechnical Engineering. [online] https://doi.org/https://doi.org/10.1016/j.jrmge.2023.07.010.

Zheng, Y., Xia, L. and Yu, Q., 2015. *Analysis of the removability and stability of rock blocks by considering the rock bridge effect*. Canadian Geotechnical Journal, 53, 150821143630006. https://doi.org/10.1139/cgj-2014-0503.

Zhu, H., Azarafza, M. and Akgün, H., 2022. *Deep learning-based key-block classification framework for discontinuous rock slopes*. Journal of Rock Mechanics and Geotechnical Engineering, [online] 14(4), pp. 1131–1139. https://doi.org/https://doi.org/10.1016/j.jrmge.2022.06.007.

APPENDIX A: THREE-SIDED BLOCK DATA QUALITY

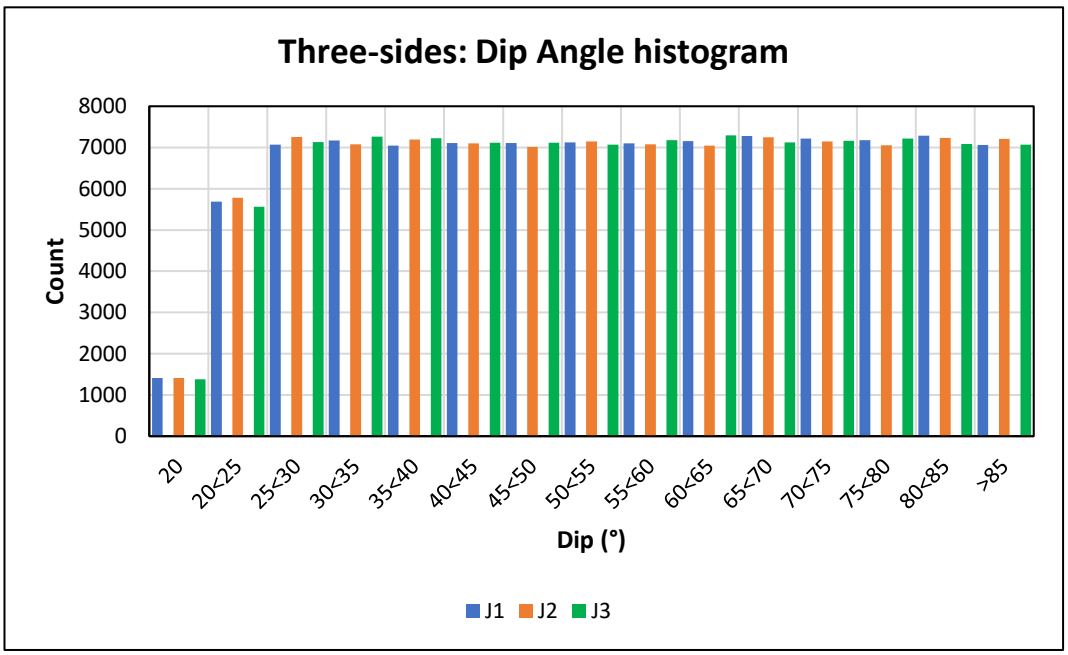


Figure A - 1: Three-sided dip angle histogram

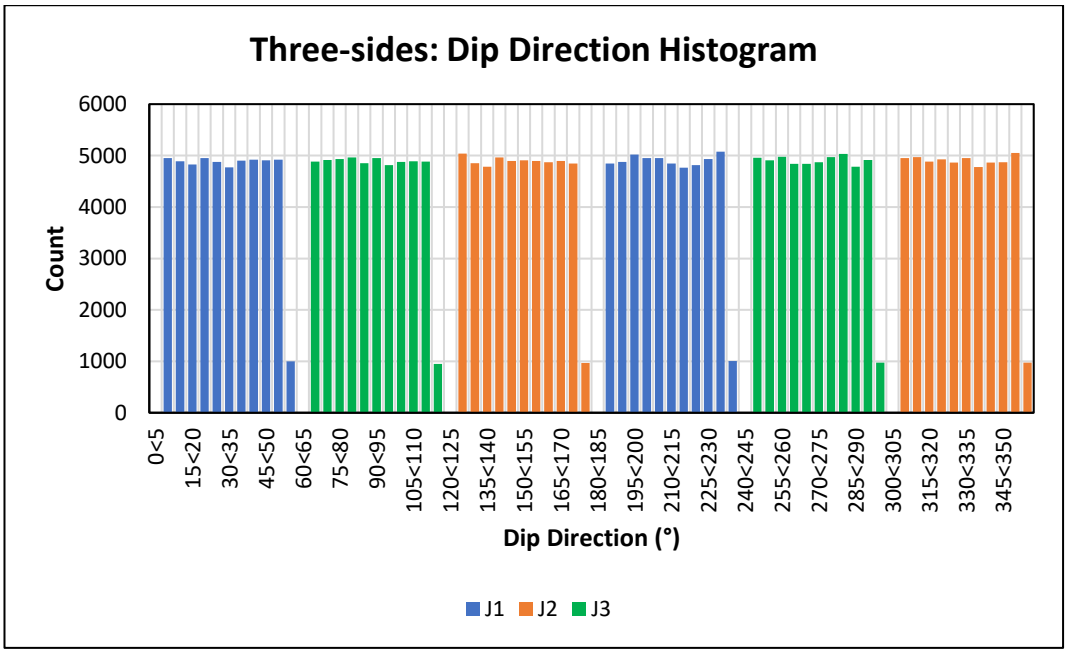


Figure A - 2: Three-sided dip direction histogram

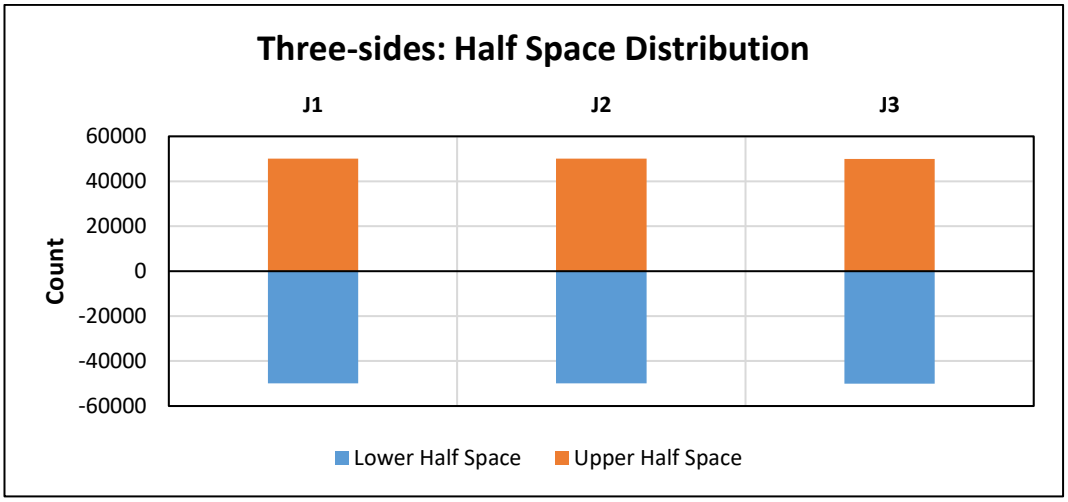


Figure A - 3: Three-sided half space distribution

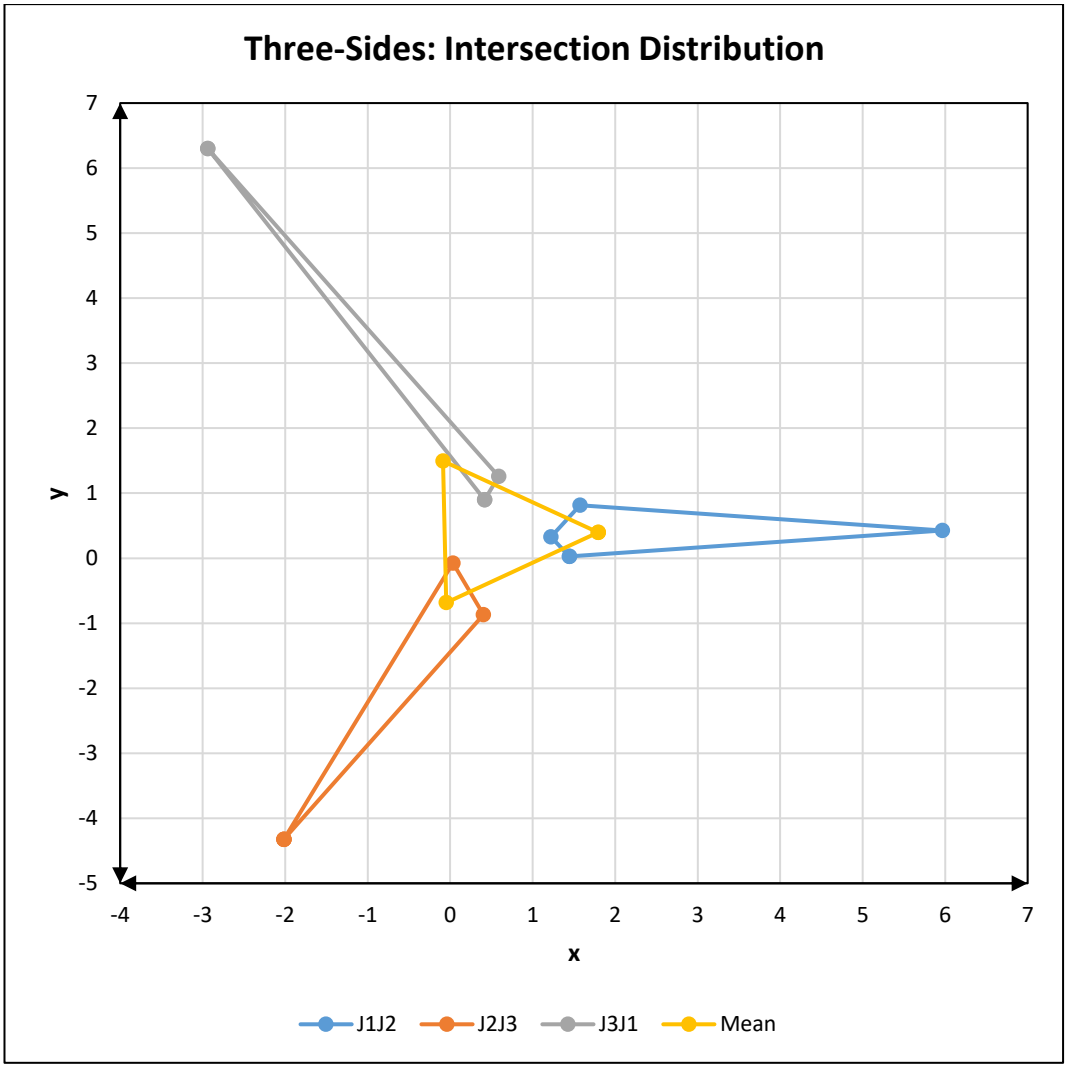


Figure A - 4: Three-sided intersection distribution

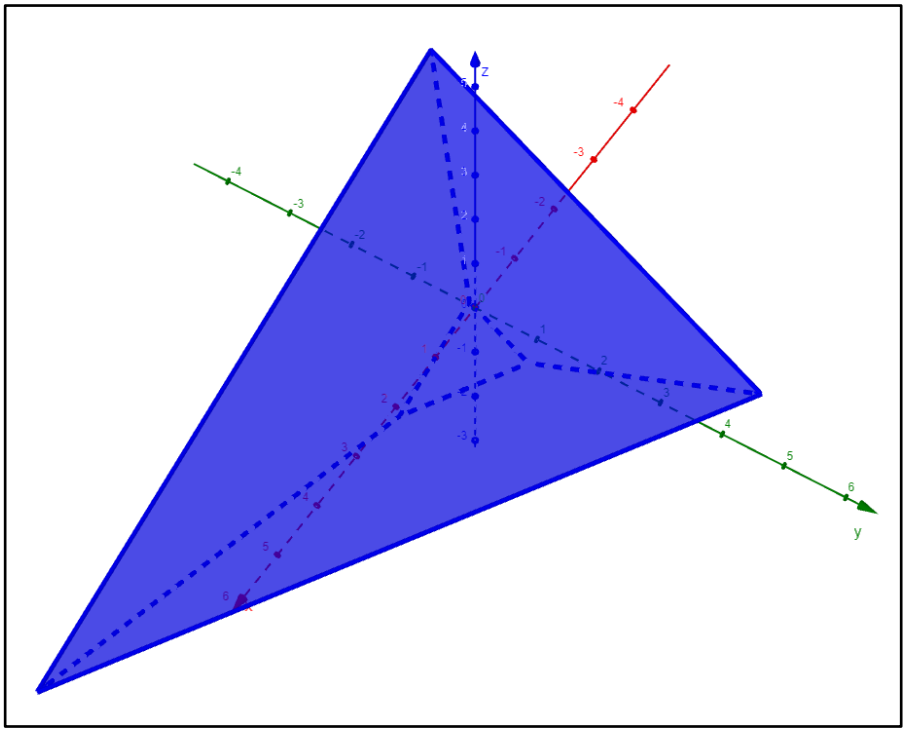


Figure A - 5: Three-sided non-removable block

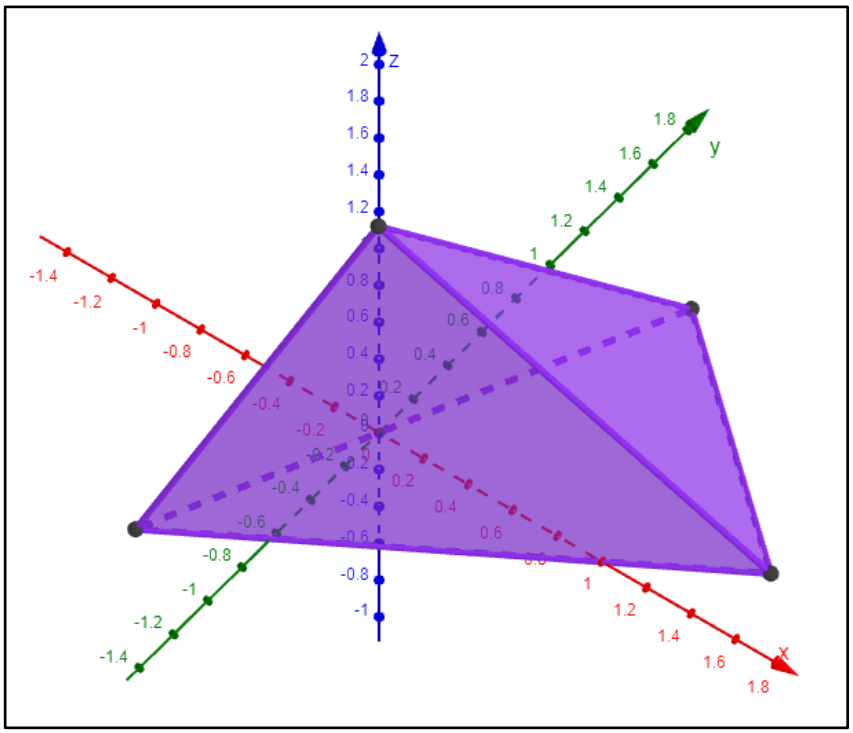


Figure A - 6: Three-sided removable block

APPENDIX B: FOUR-SIDED BLOCK DATA QUALITY

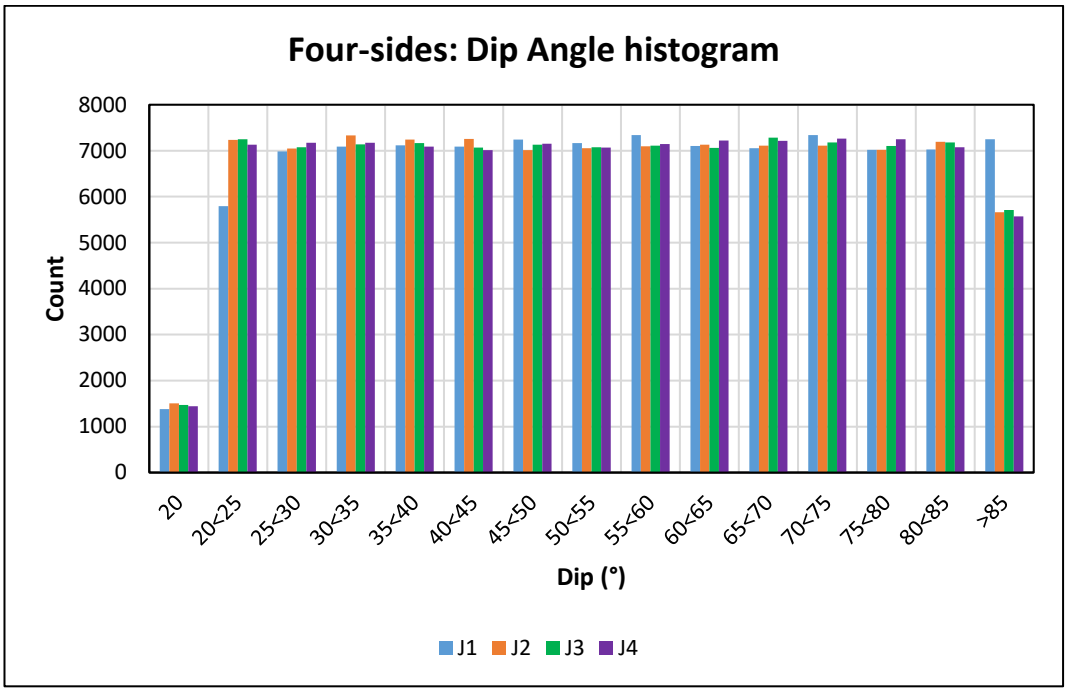


Figure B - 1: Four-sides dip angle histogram

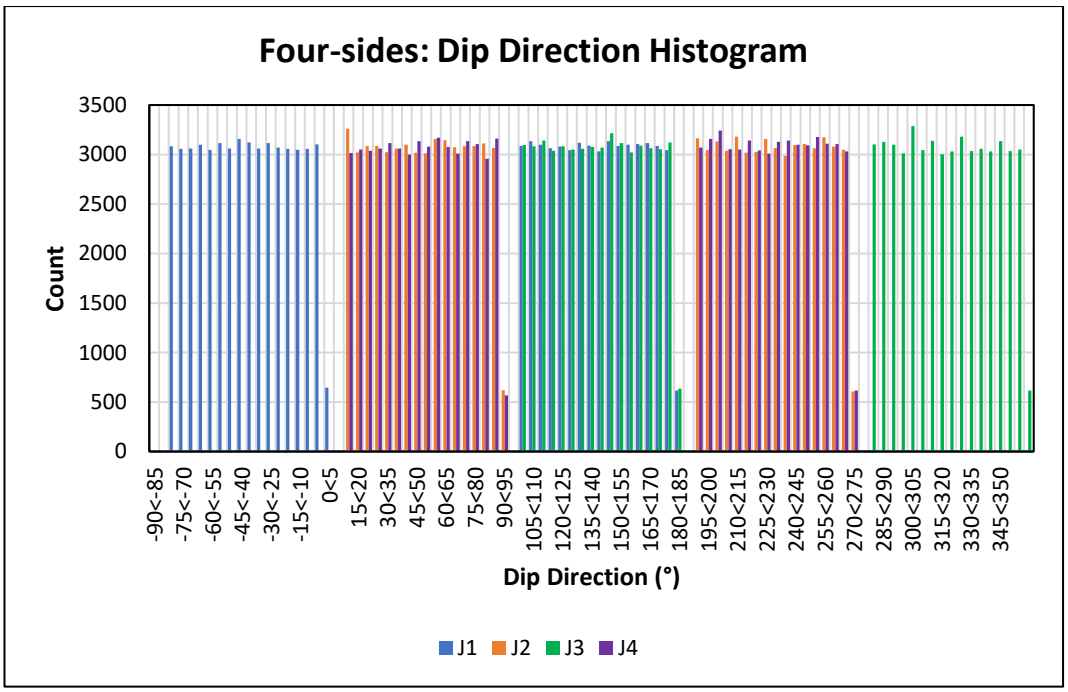


Figure B - 2: Four-sides dip direction histogram

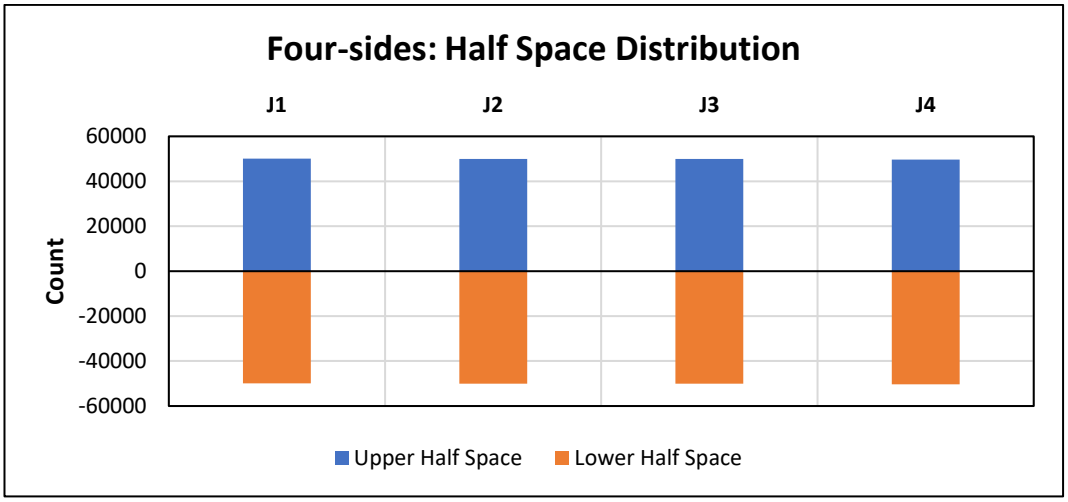


Figure B - 3: Four-sides half space distribution

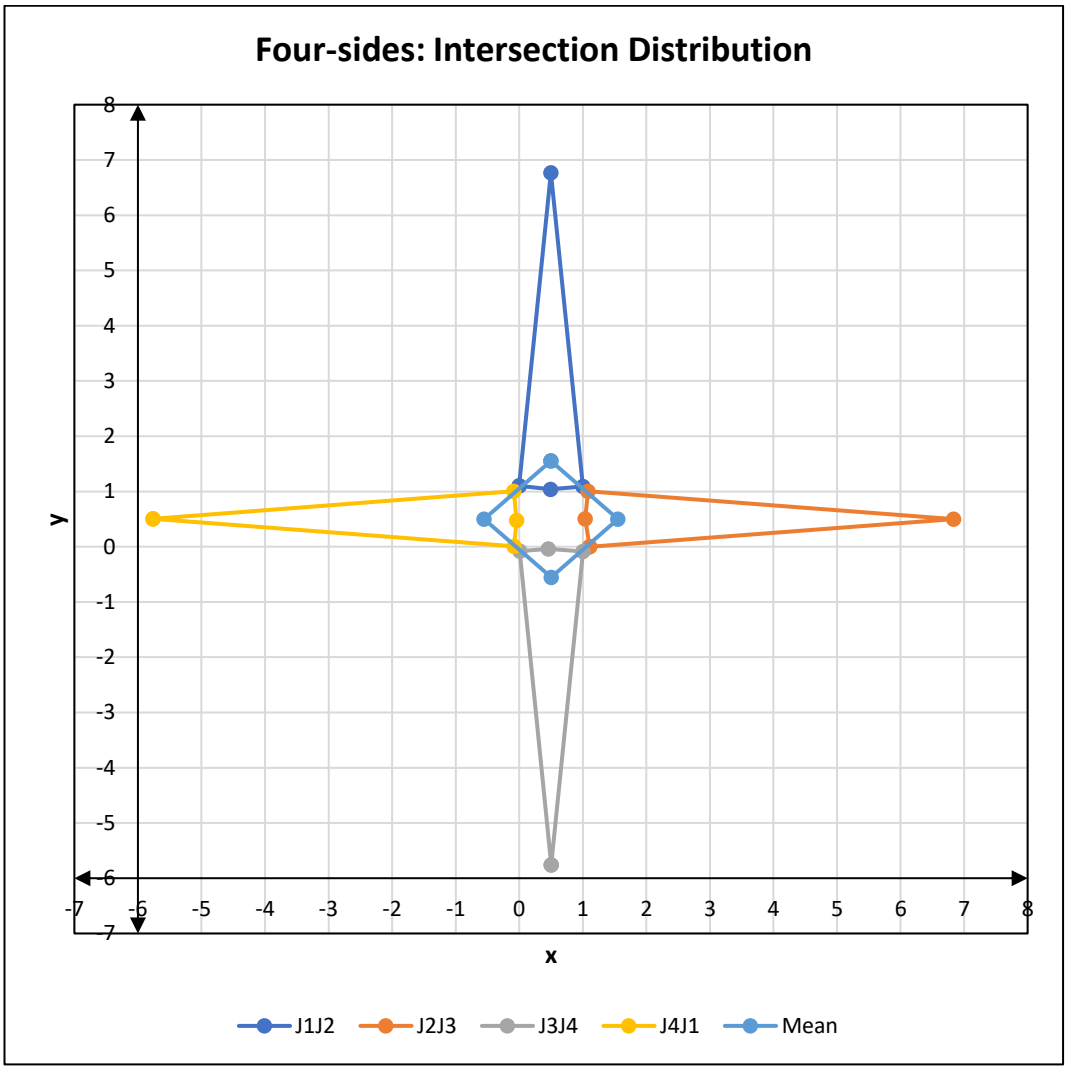


Figure B - 4: Four-sided intersection distribution

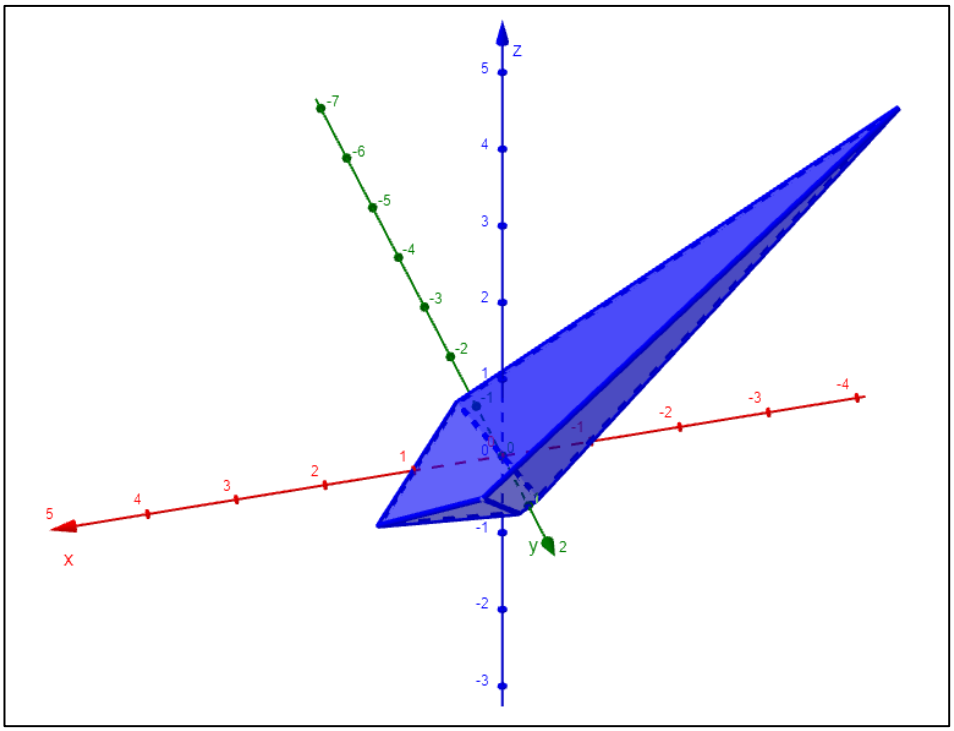


Figure B - 5: Four-sided non-removable block

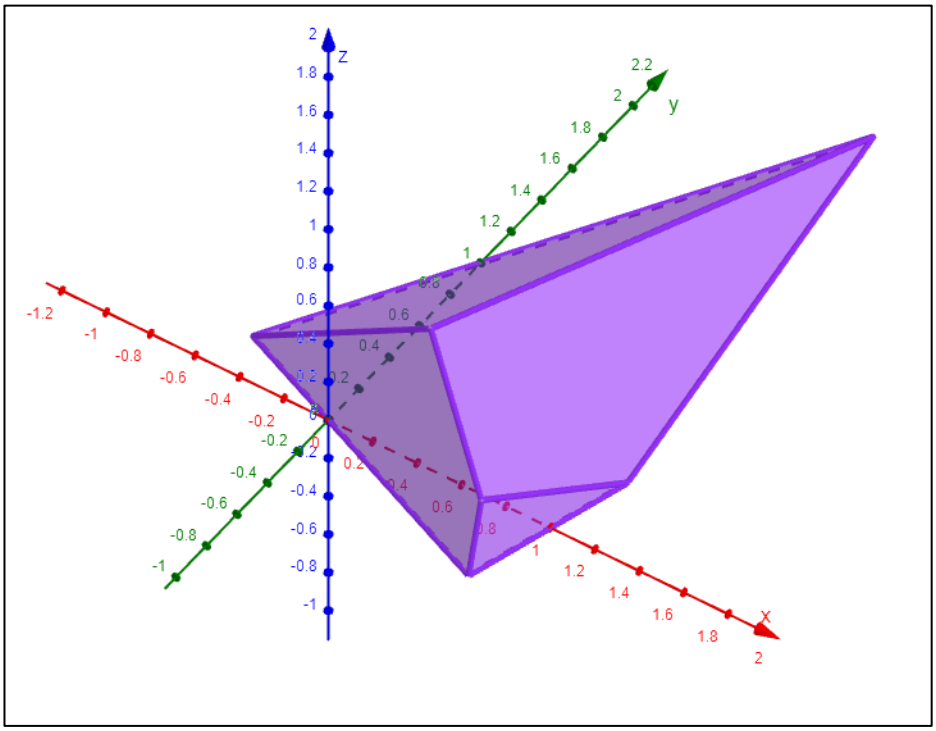


Figure B - 6: Four-sided removable block

APPENDIX C: FIVE-SIDED BLOCKS DATA QUALITY

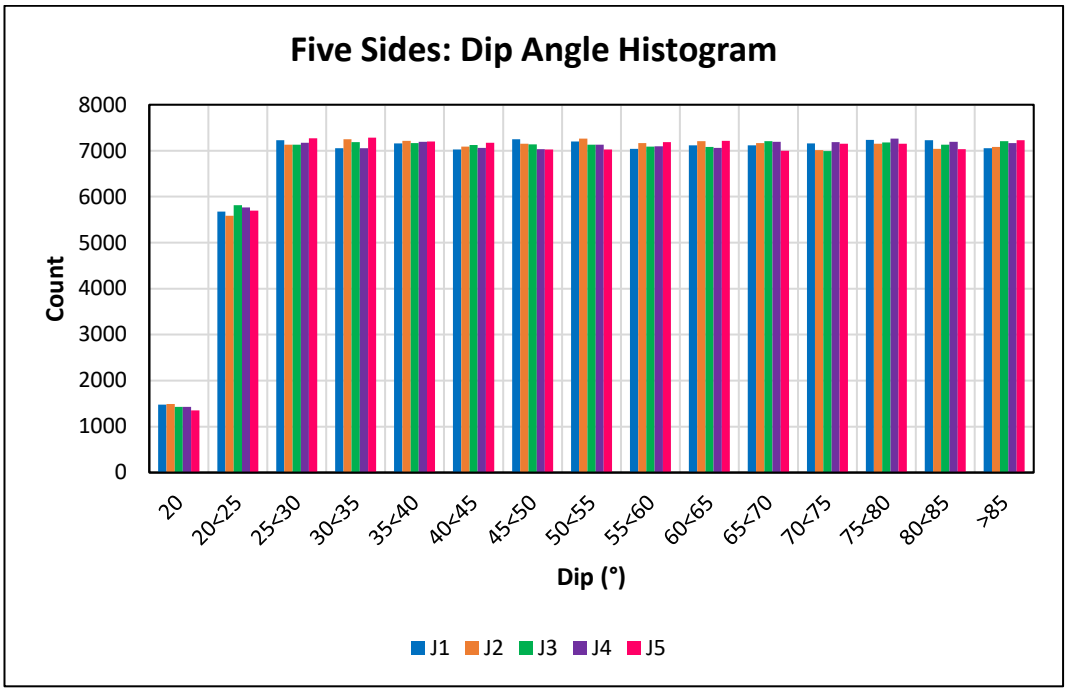


Figure C - 1: Five-sided dip angle histogram

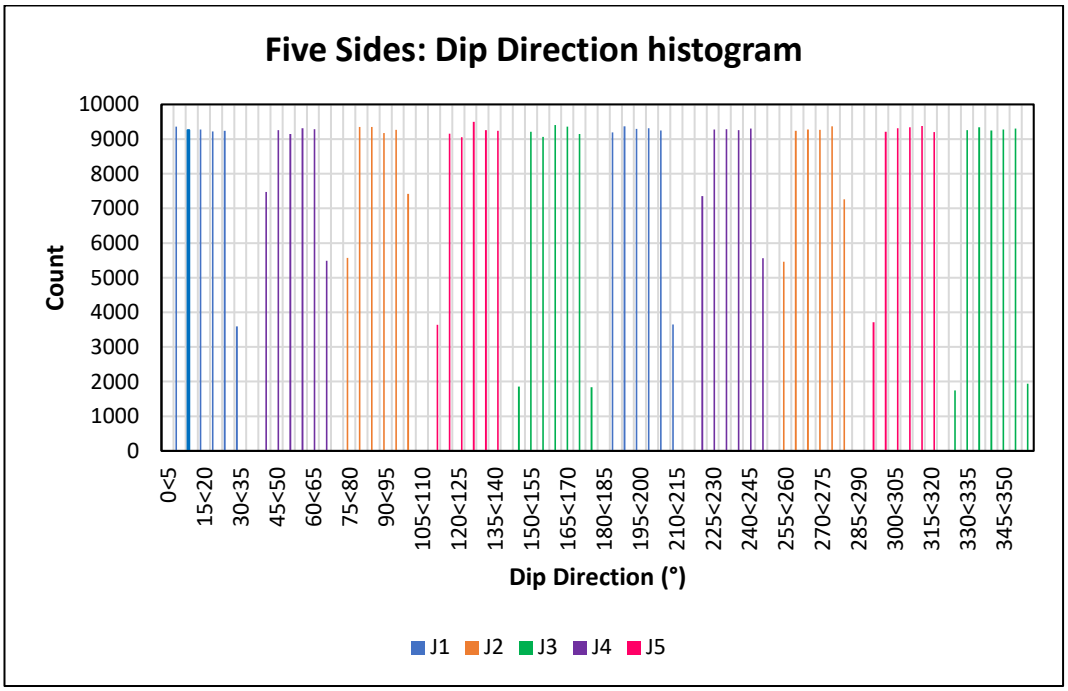


Figure C - 2: Five-sided dip direction histogram

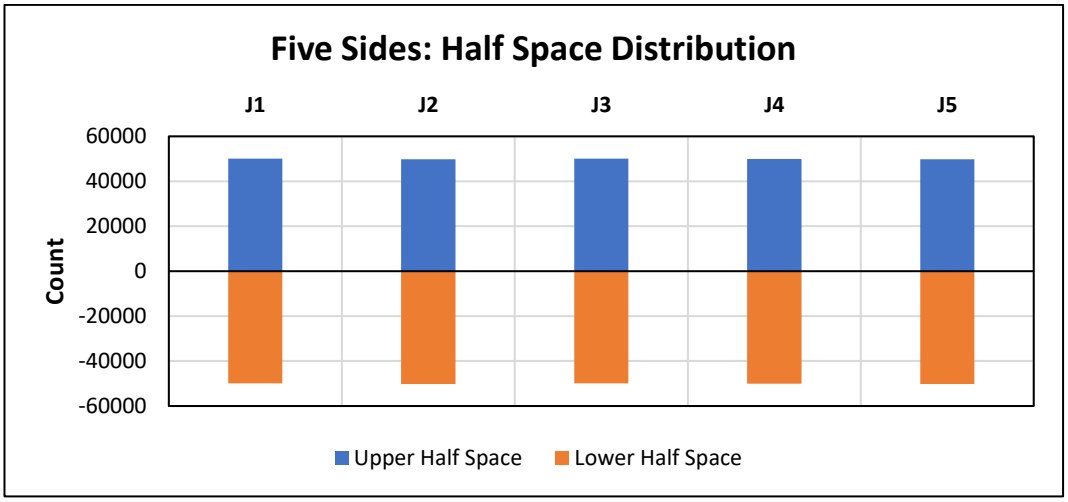


Figure C - 3: Five-sided half space distribution

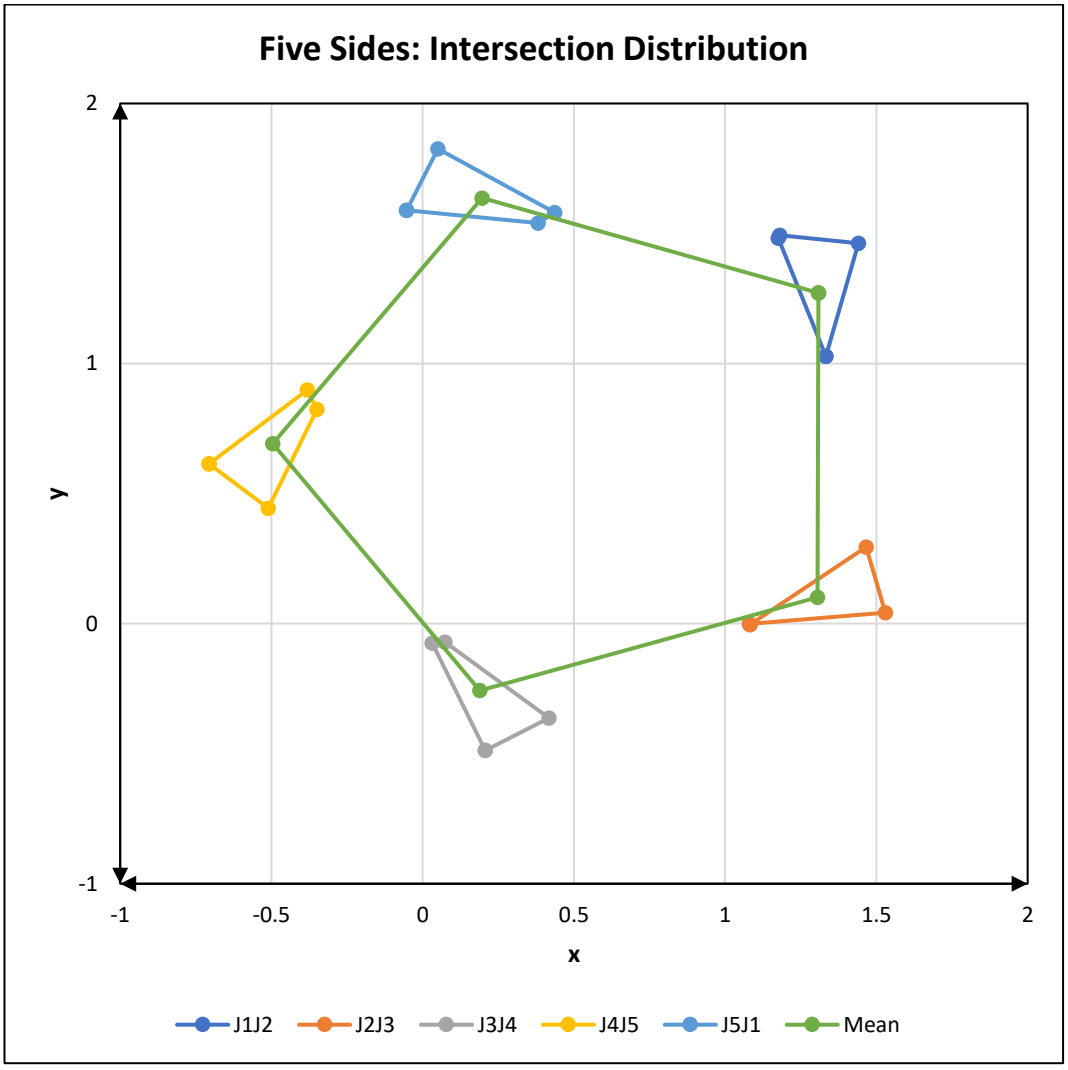


Figure C - 4: Five-sided intersection distribution

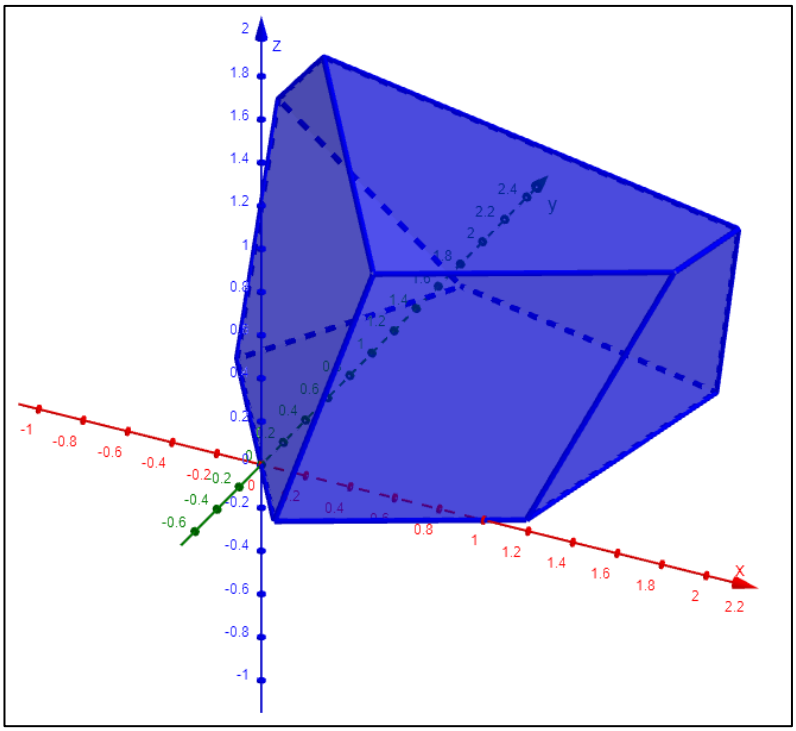


Figure C - 5: Five-sided non-removable block

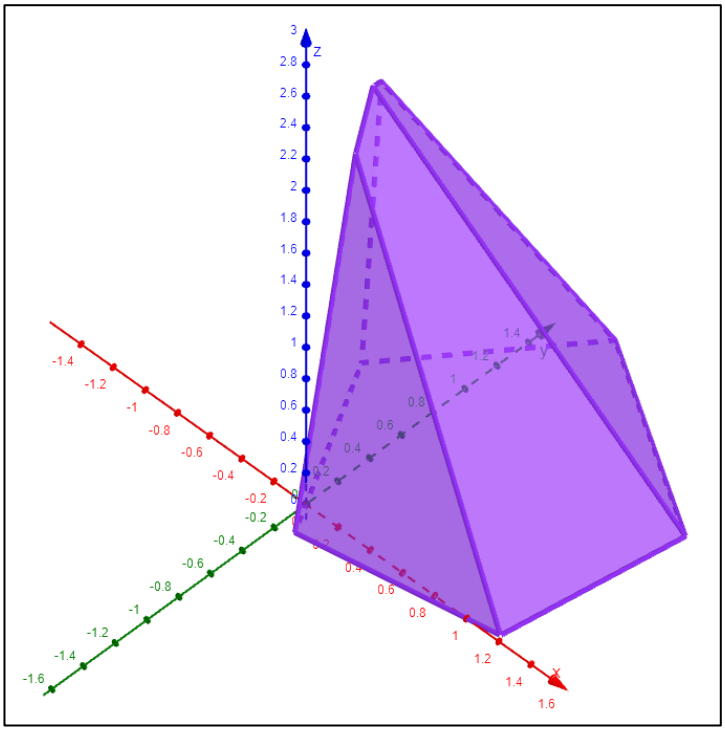


Figure C - 6: Five-sided removable block